Hydroclimatic Variability: South Saskatchewan River Basin

Final Report
March 26, 2010

Prairie Adaptation Research Collaborative
University of Regina

CONTENTS

.

.

EXECUTIVE SUMMARY

Introduction

Recent national and provincial assessments of climate change impacts and adaptation have identified shifts in the distribution of water resources, between seasons, years and watersheds, as the major risk from climate change in the Prairies region. Adaptation to avoid or reduce adverse impacts on communities, economies, and managed ecosystems requires knowledge of trends and variability in surface and soil water balances. Nearly all of the existing information on future climate and water supplies is in the form of change scenarios, that is, the expected shift in mean conditions from the recent past (usually 1961-90) to a future 30-year period, typically 2010-39, 2040-69 or 2070-99. Knowledge of expected future average conditions for a 30-year period is important and useful information; however, it is insufficient to address most of the climate impact and adaptation issues in the Prairie Provinces. The major challenge from climate change in our region is not a shift in average climate but rather the amplification of climate extremes and departures from average conditions; excessive moisture and drought. The mean water balance over a 30-year period may never exist since it is simply a central tendency or average of 30 years of annual values. While the direction and amount of change in total water balance are key data, the important information from a water management perspective is how will this change be realized since change in the hydroclimate system is not linear or incremental? That is, how will water levels fluctuate around the trending mean? What will be the severity and frequency of wet and dry years? Without knowledge of the future distribution of water among years, decades and watersheds, most decision makers will have limited technical capacity to address adaptation options, adaptive management practices and appropriate policy for planned adaptation to climate change.

Outputs from a Global Climate Model (GCM) can be used to generate a time series of a future water balance. However each run of each climate model produces a different time series; the only similarities among them are statistical properties, the mean and the variance. One approach to projecting future variability is to derive probabilities of critical water levels from a large number of climate model simulations. An alternative to this purely probabilistic approach is to understand the drivers of internal climate variability and how these drives or teleconnections will be affected by a warmer atmosphere and oceans. This approach involves the analysis of instrumental and long proxy hydrometric records to establish the nature and causes of trends and variability. A model that simulates the interannual variability in recorded streamflows from the climate drives (predictors) of hydroclimatic variability can then be used to simulate the variability of future streamflows by driving the model with climate indices derived from GCMs.

This report documents the application of these methods to river gauges in the South Saskatchewan River Basin (SSRB). This report is in four parts following the stages of the analysis as outlined above. Part 1 is this Executive Summary of the approach and results. Part 2 is an analysis of long-term hydroclimatic variability based on the reconstruction of the streamflow in the SSRB for the past 600 from a network of tree-ring chronologies. Part 3 is the analysis of the instrumental gauge records to address the question whether the observed trends and variability represent natural variability, global warming trends or other human impacts. Parts

2 and 3 of this report have been published (Axelson et al. 2009; St. Jacques et al., 2010, respectively). Therefore with this report we include the published papers that have benefited from rigorous peer-review. Part 4 documents the just completed projection of future river flows in the SSRB based on the information derived from Part 2 and 3, and output from a series of GCM experiments. Following are summaries of each stage of the project and part of the report.

New reconstructions of streamflow variability in the South Saskatchewan River Basin from a network of tree ring Chronologies

In western Canada short instrumental records limit the detection of long-term hydrological variability. To extend the historical record, we collected 14 new moisture-sensitive tree ring chronologies and reconstructed the average October through September (water year) flow of the Oldman (1618–2004) and South Saskatchewan (SSR) (1400–2004) rivers. The tree ring models accounted for 37% and 43% of the instrumental variance, respectively. Because much of the unexplained variance in the calibration period is the underestimation of high flows, we have more confidence in the interpretation of the low flows which consistently correspond to narrow tree rings, capturing the timing and duration of drought. While the 20th century is representative of drought frequency over the long term, there are droughts of greater severity and especially duration in the proxy record.

The 605 years of reconstructed flow represent an important historical context for institutional worst-case scenarios which rely on instrumental records that are generally shorter than the low-frequency variability captured by our tree ring records. Spectral analysis of the proxy hydrometric records revealed a highly significant multidecadal (~ 65 years) component of variability in both reconstructions together with significant variability at interannual time scales (2–6 years) in the El Nino-Southern Oscillation (ENSO) band. The multidecadal variability in the tree ring reconstructions of streamflow provide an alternative interpretation of trends in gauge records that are decades in length. The longer perspective, provided by tree ring reconstructions of stream flow, can address the degree to which recent trends represent components of long-term low-frequency variability in the regional hydroclimate.

For the 387-year Oldman River record, the longest wet interval occurred from 1897 to 1913, the period when most Euro-Canadian settlers arrived in the region; and the longest dry interval was from 1862 to 1876, shortly prior to settlement. For the South Saskatchewan River, the longest wet interval was from 1825 to 1841 and longest dry interval was during 1552 to 1571. The SSR record extending to 1400 is characterized by low flows from the 1470s to the 1570s, with extreme drought in the 1560s. The earliest severe hydrological drought (lowest 10th percentile) common to both reconstructions occurred from 1717 to 1721, when at least one of these years was ranked as one of the ten driest years. Both reconstructions had only one drought year in the post-settlement (instrumental) period; 1985 (first) and 1919 (sixth) in the Oldman River and SSR records, respectively. Although the 1930s are considered one of the worst droughts periods in memory in western North America, it does not appear as an extreme drought in either reconstruction.

The demand for the water resources of the SSRB suggests that an awareness of interannual to multidecadal variation in hydroclimate is essential for water resource management and planning

in the basin. This study has clearly documental long-term low-frequency variability in regional hydroclimate that must be considered in any interpretation of recent trends in gauged streamflow and projections of future water supplies in the basin. A significant decreasing trend in the annual flow of the South Saskatchewan River is documented in recent analyses of gauge records. Much of this declining flow can be attributed to water storage, diversion and consumption but it is also consistent with projections of future flows derived by coupling hydrologic models and climate change scenarios. Future raw water supplies will be determined by global warming impacts on the hydrology of the headwater basins and imposed on the interannual to multidecadal variability revealed in our tree-ring reconstructions.

Northern Rocky Mountain streamflow records: global warming trends, human impacts or natural variability?

The ~60 year Pacific Decadal Oscillation (PDO) is a major factor controlling streamflow from the Rocky Mountains, causing dryness during its positive phase, and wetness during its negative phase. If the PDO's influence is not incorporated into a trend analysis of streamflows, it can produce detected declines that are actually artifacts of this low-frequency variability. Further difficulties arise from the short length and discontinuity of most gauge records, human impacts, and residual autocorrelation.

We analyze southern Alberta and environs instrumental streamflow data, using void-filled datasets from unregulated and regulated gauges and naturalized records, and Generalized Least Squares regression to explicitly model the impacts of the PDO and other climate oscillations. We conclude that streamflows are declining at most gauges due to hydroclimatic changes (probably from global warming) and severe human impacts, which are of the same order of magnitude as the hydroclimate changes, if not greater. Surface water supplies are indeed becoming scarcer in southern Alberta even when the confounding effects of the PDO and other sources of natural variability are factored out. We found fifteen significant decreasing linear trends in the streamflow records, versus only two increasing linear trends and seven null trends. There were no strong differences between the eight unregulated headwater gauges with three detected declining trends, and the eight naturalized flow records (at downstream gauges), five with declining trends, although the number of available long records is limited. There was a geographical pattern, with the gauges in the Bow River watershed more likely to show declining flow. The current year PDO or a lead or lag was the explanatory variable that appeared most consistently in the optimum predictor set, with only two exceptions: the actual flows of the Elbow and Spray Rivers. The PDO's strong influence was also shown by individual stream records divided into the four phases of the PDO over the past century: higher flows in the cold phases (1900-1924 and 1946-1976) and lower flows during the warm phases (1925-1945 and 1977-2007). Low-pass filtered streamflow data comprised a large percentage (a mean of 46.8%) of the total variability in annual flows, confirming that low-frequency variance is an important component of the hydroclimatic variability.

Because we explicitly modelled the influence of the PDO, and used longer records that include at least one full PDO cycle, we could factor out the PDO's effect and conclude that the detected declining trends in surface water supplies are due to hydroclimatic changes (probably from global warming) and/or severe human impacts, and are not merely PDO phase artifacts. The effect of human impacts was strong. More actual flow records showed declines than did their

corresponding naturalized records; and declines were greater in actual flows than in naturalized flows. The declines in the naturalized and unregulated gauge records reflect only hydroclimatic changes, whereas fluctuations in the actual regulated gauge records reflect both global warming effects and direct human impacts. Hence, human impact could be estimated by the difference in annualized decline rates between the actual and naturalized flows. The human impacts were typically of the same order of magnitude as the hydroclimate changes, if not greater.

According to this analysis of instrumental streamflow records, future water availability in southern Alberta does not look encouraging, even without considering the expected increasing water demands of a growing economy and population. The PDO is shown to have a major impact on present-day surface water supplies. The PDO's regional importance is further underlined by tree-ring inferred streamflow reconstructions for the South Saskatchewan River Basin which show a PDO-like signal for the past six centuries, including prolonged 20-35 year low-flow regimes (Axelson et al., 2009). Because of its influence on Alberta streamflow, the status of the PDO in a warmer world under anthropogenic climate change is of serious interest. Regardless of the exact relationship between the PDO and ENSO, the change to a more El Niño dominated world is expected to have major impacts (probably decreases) on southern Alberta river flow, given its strong connection to the PDO.

Projected Southern Alberta River Discharges: 2010-2050

The 20th century hydroclimatology of southern Alberta is heavily influenced by recurring large-scale climate patterns: the Pacific Decadal Oscillation (PDO), the El Nino-Southern Oscillation (ENSO), and the Arctic Oscillation/North Atlantic Oscillation (AO/NAO). Hence, southern Alberta river discharge variability can be successfully modeled by regression techniques using these climate indices as predictors. We developed generalized-least-squares (GLS) regression equations which captured a large portion of streamflow variability (St. Jacques et al., in press). Using archived runs from global climate models, we projected the PDO, ENSO and the NAO for the first half of the 21st century. These projected climate indices were used as inputs into the GLS regression equations, giving projected southern Alberta river discharge for the early 21st century. These projections showed declining trends in southern Alberta surface water availability for 2010-2050 and increased inter-annual variability relative to the latter half of the 20th century. This study further emphasizes that any deleterious effects of global warming on surface water supplies are only compounded by the drawdown effects of direct human impacts, which are of at least a similar order of magnitude. This is particularly illustrated by the projection of the all-model mean of the actual flow of the Oldman River at Lethbridge, an acknowledged over-allocated system, which is projected to reach nearly zero flows by mid-century.

The declining trends and the PDO terms were the most influential predictors among those examined. This study found a greater prevalence of declining significant trends than the earlier study of St. Jacques et al. (in press) on many of the same discharge records. We attribute this to our use of the later compiled and more complete HadSST2 dataset in our construction of the PDO index, which we think more accurately represents the historic North Pacific pattern of variability. St. Jacques et al. (in press) used Mantua's PDO index in their analysis which was based upon the earlier and less complete HadSST1 dataset.

Because of its influence on western Canadian river discharge, the status of the PDO in a warmer world under anthropogenic climate change is of serious interest. The ability of the current highest-resolution GCMs to project the future status of the PDO is just beginning to be examined. As far as we know, our present study is the first to explicitly project the PDO and its finding of an increase in positive phase PDO events for the early 21st century leads to concern for future surface water availability. Our analysis required that output from the each GCM was available for both the 20th century and 21st century in simultaneous runs. From an array of model experiments, we chose those that best simulate the low-frequency variability at PDO wavelengths. After comparing the GCMs temporal variability of the 20th century hindcast PDO, SOI and NAO to the observed indices, we concluded the HadCM3 and CGCM3 (T63) ranked as the top two models.

The mechanism by which the PDO, or the zonal dipole in North Pacific SSTs, affects the hydroclimatology of the Pacific Northwest and interior is thru control of the position of the sub-polar jet, which brings winter storms and precipitation, as it crosses over the edge of the continent. We presume that the same mechanism will continue to operate in the early 21st century in the presence of an increased global warming trend, as it operated in the 20th century in the presence of an increasing global warming trend in surface air temperatures and SSTs. Hence, it is reasonable to forecast the PDO by projecting the 1994-2050 residual SST anomalies from each of the GCMs onto the leading eigenvector (EOF 1) from the 1900-1993 observed SST data. However, it seems unwise to assume that this mechanism will operate as before when the global warming trend surpasses the natural North Pacific variability circa 2040-2050.

The status of ENSO in a warmer world under anthropogenic climate change will also have repercussions on southern Alberta streamflow. The majority of the most recent GCMs show that a warmer world will have relatively more El Niños by the late 21st century under the A2 emission scenario. This accords with our multi-model mean shift towards more frequent El Niños for the early 21st century for both the A1B and A2 emissions scenarios. It is unknown whether the PDO is independent of ENSO or not, and this is an active area of research. If ENSO drives the PDO, i.e., that El Niño (La Niña) drives the positive (negative) phase of the PDO, then since there will be more El Niño events under global warming, the PDO will be in its positive phase more often (which accords with this study's projections) and southern Alberta will see more frequent drier conditions. However, if the PDO is independent of ENSO, but re-enforcing interactions occur between the two oscillations, then the PDO will be in its positive phase more often and there will be more frequent El Niños, and southern Alberta will see more frequent and more severe drier conditions. Thus, regardless of the precise relationship between the PDO and ENSO, the change to a more El Niño-dominated and a more positive PDO-dominated world is expected to cause decreased southern Alberta river flow in the 21st century.

The NAO/AO is an important contributor to the Northern Hemisphere climate variability. We projected that the future climate will exhibit a more positive NAO pattern than that experienced during the observed period, which should result in drier winter conditions in southern Alberta. However, we found that our all-model 1900-1999 hindcast mean was quite different from the observed 1900-1999 mean NAO index, leading to concerns as to how well the GCMs are capturing the NAO's behaviour. We are not alone in this concern.

This work is new in terms of the attempt to simulate the near-future status of the teleconnections that are strongly linked to observed water levels in southern Alberta (St. Jacques et al., in press) and are apparent in long moisture-sensitive tree-ring records (Axelson et al., 2009). We have selected those climate models that best simulate this behaviour of the climate system. When we drive a statistical climate-streamflow model with future annual values of the climate indices, water levels in the model consistently decline. The interannual variability in water level increases in to the future relative to the variability evident in the streamflow simulations for the latter half of the 20th century, although the models produce some large departures from average flows earlier in the 20th century simulation. Large and sustained negative departures from the declining mean water levels are particularly concerning and likely represent the major challenge presented by global warming impacts on the water supplies in southern Alberta.

References

Axelson, J. N., D. J. Sauchyn, and J. Barichivich. 2009. New reconstructions of streamflow variability in the South Saskatchewan River Basin from a network of tree ring chronologies, Alberta, Canada, Water Resources Research, 45, W09422, doi:10.1029/2008WR007639.

St. Jacques, J.M., Sauchyn, D.J and Yang Zhao. 2010. Southern Alberta streamflow records: global warming trends, human impacts or natural variability? Geophysical Research Letters, 37, L06407, doi:10.1029/2009GL042045.

New reconstructions of streamflow variability in the South Saskatchewan River Basin from a network of tree ring chronologies, Alberta, Canada

Jodi N. Axelson,[1] David J. Sauchyn,[2] and Jonathan Barichivich[3]

Received 9 December 2008; revised 11 June 2009; accepted 25 June 2009; published 29 September 2009.

[1] In western Canada growing demand for water resources has increased vulnerability to hydrological drought. The near full allocation of water supplies in the Oldman and Bow River subbasins of the South Saskatchewan River Basin has resulted in a moratorium on new surface water licenses. In this region, short instrumental records limit the detection of long-term hydrological variability. To extend the historical record, we collected 14 new moisture-sensitive tree ring chronologies and reconstructed the average October through September flow of the Oldman (1618–2004) and South Saskatchewan (SSR) (1400–2004) rivers. Our SSR proxy record updates a previously published reconstruction. While the 20th century is representative of drought frequency over the long term, droughts are of greater severity and duration in the preinstrumental proxy record. A spectral analysis of the reconstructed flows revealed quasiperiodic cycles at interannual to multidecadal scales.

Citation: Axelson, J. N., D. J. Sauchyn, and J. Barichivich (2009), New reconstructions of streamflow variability in the South Saskatchewan River Basin from a network of tree ring chronologies, Alberta, Canada, *Water Resour. Res.*, *45*, W09422, doi:10.1029/2008WR007639.

1. Introduction

[2] Demand for water supplies in the Prairie Provinces of western Canada is rising with growth in population and economic activity [*Schindler and Donahue*, 2006]. This growing dependence on the water resources has increased vulnerability to hydrological drought. Prairie drought is Canada's most costly climate hazard; the drought of 2001–2002 cost the prairie agricultural sector an estimated $3.6 billion [*Wheaton et al.*, 2005] and, during the drought of 1988, energy providers sustained up to $73 million in economic losses [*McKay et al.*, 1989; *Wheaton et al.*, 1992]. Future water scarcity would be a significant constraint on economic development including expansions of irrigated lands and oil sands production.

[3] The most serious risk from recent and projected climate warming in western Canada is a shift in the amount and timing of streamflow [*Pietroniro et al.*, 2006; *Sauchyn and Kulshreshtha*, 2008]. The snow-dominated basins of midlatitudes to high latitudes are losing the advantage of a cold winter; snow and ice are the most reliable, predictable and abundant sources of spring and summer runoff [*Barnett et al.*, 2005]. Sensitivity analysis of mountain snowmelt hydrology demonstrates that regional warming shifts stream hydrographs earlier into the winter and spring at the expense of summer runoff [*Brubaker and Rango*, 1996; *Nijssen et al.*, 2001]. The earlier loss of the annual snowpack contributes to negative glacier mass balance, which is among the strongest signals of the impacts of global warming in the Rocky Mountains of western Canada [*Sauchyn et al.*, 2009].

[4] Coupled with the sensitivity of the human and natural systems to climate variability is a highly variable hydroclimate. The coefficient of variation (standard deviation divided by mean) in annual precipitation in the populated (monitored) region of Canada reaches maximum values (>25%) in the central prairies over an area roughly corresponding to the South Saskatchewan River Basin [*Longley*, 1953]. Despite documented variability over a range of time scales, from annual to decadal to millennial [*St. George and Sauchyn*, 2006; *Michels et al.*, 2007), resource management practices and policies have assumed a stationary hydrological regime. Western water use, policy and management were established during a period of fairly stable and reliable water supplies as compared to the recent past and near future [*Sauchyn et al.*, 2009]. Paradigms and practices of water management must be adjusted to manage a hydrological cycle that may be increasingly sensitive to the timing and frequency of precipitation events with less of a buffer from glacier ice and late lying snow at high elevations.

[5] The Prairie Provinces of Alberta, Saskatchewan and Manitoba share the water resources of the Saskatchewan River Basin (SRB) according to the 1969 Master Apportionment Agreement, whereby each province is allocated a percentage of the 'natural' flow from the SRB. With climate change, water managers will increasingly have to manage for conditions outside the short historical experience. Managing for the greater range of hydrologic variability evident in proxy and projected, versus gauged, hydrometric records can prepare water managers for adaptation to climate

[1]Pacific Forestry Centre, Canadian Forest Service, Natural Resources Canada, Victoria, British Columbia, Canada.
[2]Prairie Adaptation Research Collaborative, University of Regina, Regina, Saskatchewan, Canada.
[3]Climatic Research Unit, University of East Anglia, Norwich, UK.

0043-1397/09/2008WR007639$09.00

change. Centuries long tree ring reconstructions of streamflow capture hydroclimatic variability at annual to multidecadal scales [*Stockton and Jacoby*, 1976; *Meko et al.*, 1991; *Woodhouse*, 2001; *Case and MacDonald*, 2003; *Gedalof et al.*, 2004].

[6] Tree rings are well suited for hydrological reconstructions as they have annual resolution and wide distribution, and climate conditions causing decreased watershed runoff (low precipitation, high evapotranspiration) also cause decreased water potential in trees [*Loaiciga et al.*, 1993; *Meko et al.*, 1995]. Tree ring indices correlate with hydrologic variables in a range of hydroclimatic regimes [*Schulman*, 1945; *Stockton and Jacoby*, 1976; *Smith and Stockton*, 1981; *Cook*, 1985; *Cleaveland and Stahle*, 1989] and particularly with streamflow data that integrate runoff over space and among events [*Loaiciga et al.*, 1993; *Meko et al.*, 1995; *Hidalgo et al.*, 2001]. Tree ring signals are coherent over hundreds of kilometers reflecting a regional (basin) hydroclimatic signal. In western Canada, tree ring reconstructions of streamflow have been developed for the Athabasca [*Bonin and Burn*, 2005], Churchill [*Beriault and Sauchyn*, 2006], Bow [*Watson and Luckman*, 2005a], and Saskatchewan rivers [*Case and MacDonald*, 2003]. Other tree ring studies in the region have investigated lake levels in the Athabasca Basin [*Stockton and Fritts*, 1973; *Meko*, 2006] and floods in the Red River Basin [*St. George and Nielsen*, 2002a, 2002b].

[7] In this paper we present two reconstructions of mean water year flow (October through September) inferred from a network of 14 new tree ring chronologies collected throughout the upper western regions of the South Saskatchewan River Basin (SSRB). The flow of the South Saskatchewan River (SSR) was previously reconstructed by *Case and MacDonald* [2003] using tree ring chronologies from two sites in the SSRB. The two chronologies were from moisture-sensitive limber pine (*Pinus flexilis* James) at exposed xeric sites. We collected tree rings from limber pine at four sites, but also from Douglas fir (*Pseudotsuga menziesii* (Mirb.) Franco) at 10 sites, to produce robust reconstructions of the flow of the SSR and one of the main tributaries, the Oldman River. Douglas fir occupies a greater variety of sites than limber pine, and thus a network of Douglas fir chronologies encompasses a greater range of local hydroclimatic conditions throughout the upper reaches of the SSRB, where about 80% of the runoff in the entire basin is generated [*Prairie Provinces Water Board* (*PPWB*), 1962]. The larger network of tree ring sites used in this study also enables the reconstruction of streamflow at a subbasin scale, and the analysis of hydroclimatic variability among basins at interannual to multidecadal scales. Recent studies [*Rood et al.*, 2005; *Schindler and Donahue*, 2006] have examined trends in the recorded flow of the SSR and conclude or imply that global warming is causing a reduction in water supplies. The longer perspective, provided by tree ring reconstructions of stream flow, can address the degree to which recent trends represent components of long-term low-frequency variability in the regional hydroclimate.

2. Study Area

[8] The South Saskatchewan River Basin (SSRB) of Alberta and Saskatchewan (Figure 1) is Canada's largest (167,765 km^2) dryland watershed. The major subbasins (and contributions to mean annual flow) are the Bow (43%), Red Deer (18%), and Oldman (38%) River basins [*Alberta Environment*, 2002]. Highest peak annual flow occurs in the snowmelt runoff season of March through June, receding to base flow conditions in July–August [*Hauer et al.*, 1997; *Marshall and Schut*, 1999]. All of the major tributaries of the SSR have large-scale water extractions and impoundments, such that summer flows in the Oldman River are 40–60% below their historical values, and in the SSR summer flows have been reduced by 84% since the early 20th century [*Schindler and Donahue*, 2006]. More than 70% of licensed surface water withdrawals in Alberta are for irrigation [*Alberta Environment*, 2005].

3. Tree Ring and Streamflow Data

[9] Of the eleven tree ring chronologies previously collected in the SSRB (International Tree Ring Data Bank, 2006, http://www.ncdc.noaa.gov/paleo/treering.html) nine predate 1992. Given the lack of current tree ring data for the SSRB, we established a network of new tree ring chronologies for the major runoff-generating areas of the basin. Douglas fir and limber pine are common throughout the region as open canopy stands at dry sites and near the eastern edge of their range. Both species are long lived, with 800-year-old limber pine and 700-year-old Douglas fir known to occur in the SSRB [*Case and MacDonald*, 2003; *Watson and Luckman*, 2006].

[10] Tree rings were collected from at least 20 trees per site at 14 sites on low-elevation dry south and southwest facing slopes where soil moisture is limited (Table 1). The densest sampling occurred in the Oldman River subbasin, where the montane landscape, fescue prairie and well drained soils are ideal conditions for open canopy stands of long-lived and moisture-sensitive coniferous trees. In the Red Deer River Basin, on the other hand, young closed canopy forests predominate and the only suitable site we located was near the headwaters of the Red Deer and James rivers at Ya Ha Tinda Ranch (YHT) (Figure 1).

[11] Sample preparation, cross dating and chronology construction followed standard dendrochronological methods [*Stokes and Smiley*, 1968; *Cook et al.*, 1990]. Tree ring width was measured to within 0.001 mm using a 40X stereomicroscope, Velmex uniSlide digitally encoded traversing table, AcuRite III digital counter, and the measuring program J2X. Cross dating ensured that exact calendar years were assigned to every tree ring, and was verified using the program COFECHA [*Holmes*, 1983]. The program ARSTAN [*Cook*, 1985] was used to standardize the measured tree ring series using conservative detrending methods: a negative exponential curve, which removes the juvenile biological growth trends in the tree ring series; or a cubic smoothing spline, a low-pass digital filter with a 50% frequency response cutoff, where the cutoff is the frequency at which 50% of the amplitude of the signal is retained [*Cook et al.*, 1990]. Chronologies ranged in length from 290 to 786 years (Table 1). Where individual chronologies were used as predictors of streamflow, the length of each chronology was limited to the segment with an expressed population signal (EPS) $\geq$0.85, minimizing inflation of variance associated with decreasing sample size [*Wigley et al.*, 1984; *Briffa and Jones*, 1990]. The standardized ring width series of various lengths were

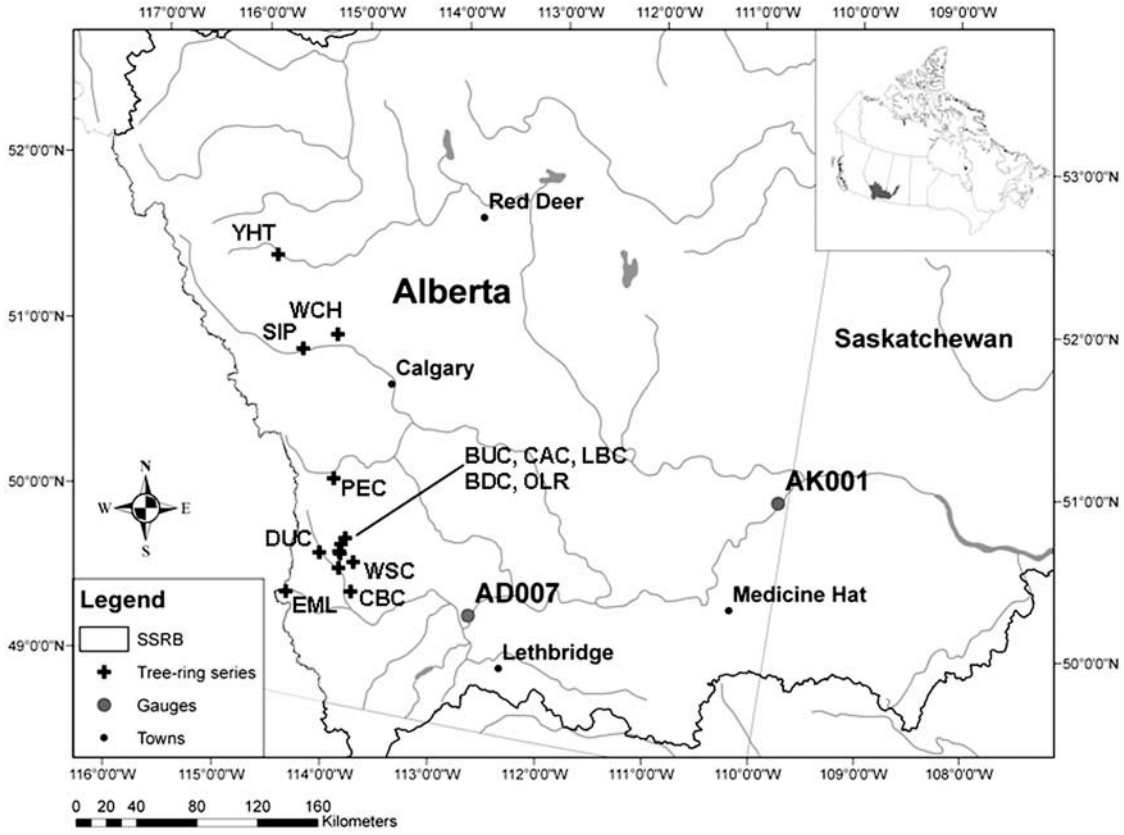

Figure 1. The South Saskatchewan River Basin (SSRB) in the Prairie Provinces of Alberta and Saskatchewan (top right inset) and locations of the tree ring chronologies and streamflow gauges in the major runoff-generating subbasins of the SSRB.

averaged for each site, using a mean value function that minimizes the effect of outliers [*Cook et al.*, 1990], producing a dimensionless stationary index time series with a defined mean of 1.0 and a relatively constant variance.

[12] Streamflow data for the SSRB were provided by Alberta Environment who derived naturalized flows from streamflow records, reservoir data, recorded and estimated irrigation withdrawals, and climate data using the Streamflow Synthesis and Reservoir Regulation (SSARR) model from U.S. Army Corps of Engineers [*Alberta Environment*, 1998]. These natural flow data for the period 1912–2001 are suitable for water management planning on the scale of the SSRB [*Alberta Environment*, 1998]. We focused on two hydrometric gauges, which integrate streamflow at different spatial scales: (1) the Oldman River near Lethbridge, Alberta (ID 05AD007), and (2) the South Saskatchewan River below the confluence with the Red Deer River, 16 km west of the Alberta-Saskatchewan border (ID 05AK001) (Table 2).

Table 1. Properties of New Tree Ring Chronologies Sampled in the South Saskatchewan River Basin, Alberta, Canada

Site Name	Code[a]	Species[b]	North Latitude	West Longitude	Elevation (m)	Number of Dated Samples	Chronology Interval	Interseries Correlation	Mean Sensitivity	Year EPS >0.85
Beaverdam Creek	BDC	PsMe	49°55′	114°12′	1661	42	1482–2004	0.736	0.363	1584
Burto Creek	BUC	PsMe	50°1′	114°11′	1536	21	1442–2004	0.681	0.332	1605
Callum Creek	CAC	PsMe	49°59′	114°12′	1677	45	1513–2004	0.744	0.310	1596
Cabin Creek	CBC	PsMe	49°42′	114°1′	1395	39	1373 –2004	0.791	0.425	1440
Dutch Creek	DUC	PsMe	49°54′	114°24′	1648	42	1618–2004	0.808	0.353	1639
Emerald Lake	EML	PiFl	49°37′	114°38′	1384	39	1450–2004	0.602	0.291	1688
Little Bob Creek	LBC	PsMe	49°56′	114°13′	1602	47	1493–2004	0.775	0.399	1607
Oldman River	OLR_1	PiFl	49°50′	114°11′	1458	60	1218–2004	0.608	0.419	1436
Oldman River	OLR_2	PsMe	49°50′	114°11′	1458	21	1490–2004	0.736	0.479	1577
Pekisko Creek	PEC	PiFl	50°22′	114°24′	1515	36	1563–2004	0.624	0.358	1640
Stoney Indian Park	SIP	PsMe	51°7′	114°58′	1300	21	1597–2003	0.788	0.354	1698
Wildcat Hills	WCH	PsMe	49°53′	114°3′	1351	35	1341–2004	0.863	0.499	1399
West Sharples Creek	WSC	PsMe	51°15′	114°40′	1575	63	1525–2004	0.767	0.374	1589
Ya Ha Tinda	YHT	PiFl	51°40′	115°25′	1529	12	1711–2001	0.477	0.230	1712

[a]Chronologies referred to by abbreviations herein.
[b]Species coded as follows: PIFL, Limber pine (*Pinus flexilis*); PSME, Douglas fir (*Pseudotsuga menziesii*).

Table 2. Information on Hydrometric Gauges in the South Saskatchewan River Basin, Alberta, Canada

Gauge ID"05"	Gauge Name	North Latitude	West Longitude	Gross Drainage Area (km^2)	Length of Record
AD007	Oldman River near Lethbridge	49°42′	112°52′	17,031	1912–2001
AK001	South Saskatchewan River at Hwy. 41	50°44′	110°5′	66,000	1912–2001

These annual streamflow time series have a Gaussian frequency distribution according to a robust nonparametric Lilliefors test of normality.

4. Methods of Streamflow Reconstruction

[13] The 14 tree ring chronologies were examined for correlations with climate and streamflow data to restrict the pool of predictors to those with a physical relationship to hydrologic variability. Correlation coefficients were calculated between residual chronologies [*Cook*, 1985] and mean monthly temperature and total monthly precipitation, using the full record from Pincher Creek, Alberta (1895–1962), in the year t and in $t - 1$ for July and August, and between the standard, residual and arstan chronologies [*Cook*, 1985] and average monthly, annual, and water year flows, using the naturalized streamflow data for the period 1912 to 2001.

[14] Principal components analysis (PCA) was used to reduce the tree ring indices to a set of independent predictors for chronologies from the Oldman River subbasin. Chronologies were grouped into two common periods: 1400–2004 (2 chronologies) and 1618–2004 (8 chronologies). Principal components (PCs) were extracted using a covariance matrix, where no more than three components were retained for further analysis. Limiting the number of potential predictors minimizes the probability of overfitting the regression model.

[15] Multiple linear regression was used to estimate streamflow from a set of potential tree ring predictors, index chronologies and PCs, for the growth year and at forward lags of 1, 2 and 3 years. The lagged predictors account for current conditions that affect tree growth in succeeding years [*Fritts*, 1976]. Reconstruction models were calibrated using a forward stepwise procedure with a cross-validation stopping rule. They were validated using a cross-validation leave-*n*-out method, where observations are left out sequentially through the length of the streamflow record allowing maximum use of the data [*Hughes et al.*, 1982].

[16] For the calibration period (1912–2001) we reported the strength of the regression models using the adjusted R^2, which quantifies the explanatory power of the regression and accounts for lost degrees of freedom [*Fritts*, 1976]. For the verification period we used the reduction of error (RE) statistic, a rigorous measure of association between a series of actual values and their estimates. The theoretical limits of the RE range from a maximum of +1 to negative infinity. Any positive value indicates that the model has some predictive capacity [*Fritts*, 1976; *Fritts et al.*, 1990]. The F level of the regression model was computed as a goodness-of-fit test. The standard error (SE) and root-mean-square error of validation ($RMSE_v$) are measures of the uncertainty in predicted values over the calibration period and validation period, respectively. Both error terms have the same units as the predictand so are used as a measure of uncertainty in the regression estimates. Regression residuals were tested for autocorrelation using the Durbin-Watson test [*Ostrom*, 1990]. The mean variance inflation factor (VIF) was calculated to identify multicollinearity in the matrix of predictor values [*Haan*, 2002].

[17] The hydroclimatic variability inherent in the streamflow reconstructions was characterized by the timing and frequency of moderate and extreme hydrological drought, defined as reconstructed flows in the lowest 25th and 10th percentiles, respectively, and by the main modes of variability identified using a multitaper method (MTM) of spectral analysis [*Mann and Lees*, 1996] and continuous wavelet transform (CWT) analysis [*Grinsted et al.*, 2004]. The MTM is a powerful and widely used nonparametric method of spectral estimation providing high resolution while minimizing spectral leakage and reducing the variance of spectral estimates by using orthogonal tapers [*Ghil et al.*, 2002]. It is particularly well suited for short and noisy time series. With a frequency resolution suitable for resolving distinct climate signals, and improved spectral estimation properties over classical methods, the MTM has been widely applied to instrumental records of atmospheric and oceanic variables. We implemented MTM using the SSA-MTM Toolkit available at http://www.atmos.ucla.edu/tcd/ssa/. The CWT analysis is a powerful tool for the identification of nonstationary signals because it decomposes the time series into frequency components. Most traditional mathematical methods that examine periodicities in the frequency domain, such as Fourier analysis, have implicitly assumed that the underlying processes are stationary in time. Wavelet transforms expand time series into time frequency space and can therefore find localized intermittent periodicities [*Grinsted et al.*, 2004].

5. Results

[18] Residual tree ring chronologies were significantly ($p < 0.05$) and positively correlated to precipitation and negatively correlated to temperature (Figure 2). The correlation with precipitation was strongest in previous August and the current spring season (May, June, July). Seven chronologies, two limber pine and the five highest elevation Douglas fir chronologies (1536 to 1677 m asl), were significantly and positively correlated to late fall and winter (November and February) precipitation, but averaged across all chronologies these correlations failed to meet the 95% confidence threshold (Figure 2). The correlation between temperature and tree ring width was predominately negative and strongest in June, July and September of the current year (Figure 2). Correlations with streamflow data (results not shown) were significant ($p < 0.05$) for all flow observation intervals: monthly, annual and water year. Standard chronologies and average water year (October–September) flows were most strongly correlated ($r = 0.30$ to 0.61; $p < 0.05$). Of the 14 potential predictor tree ring chronologies, 11 exhibited significant correlations with hydroclimatic variables; the three chronologies (EML,

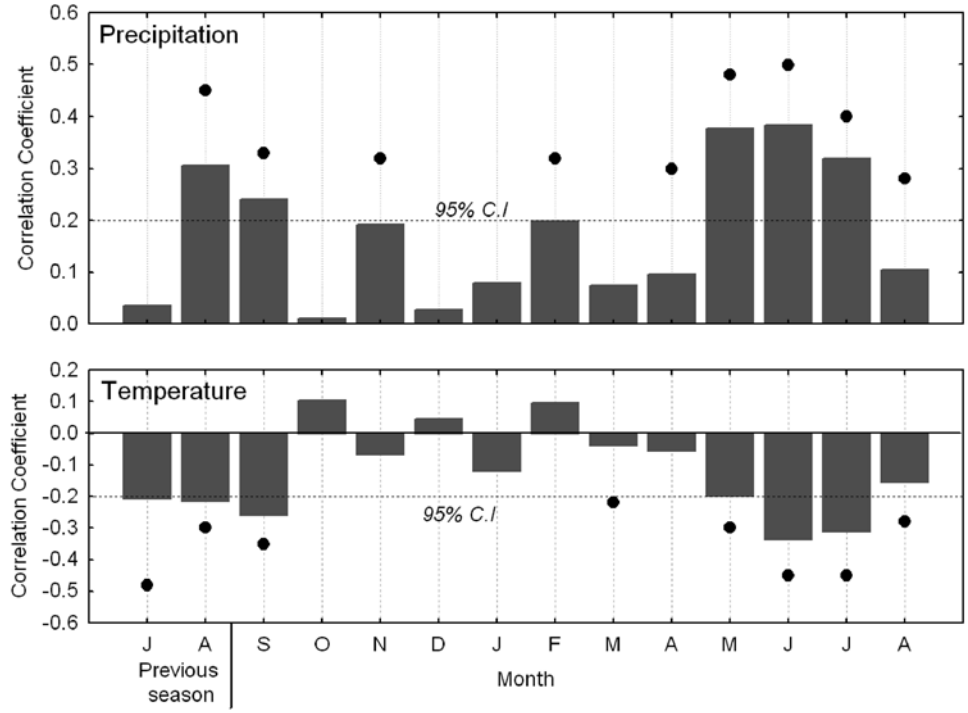

Figure 2. Average (solid bars) and maximum (dots) correlation coefficients between tree ring width indices and monthly total precipitation (mm) and mean temperature (°C) for the period 1895–1962, the length of the record from Pincher Creek, Alberta. The dotted line is the 95% confidence interval.

OLR2 and YHT) that did not were removed from the pool of predictors.

[19] The PC data sets from the Oldman River subbasin were used in conjunction with the standard chronologies to reconstruct streamflow. For the 1400–2004 common period two PCs were retained (604-PC1 and 604-PC2) and accounted for 84.3% and 15.6% of the variance in standardized tree ring width. For the 1618–2004 common period, one PC was retained (386-PC1) accounting for 77.7% of the variance (Table 3).

[20] We reconstructed average water year flow for the Oldman River at Lethbridge (AD007) and the South Saskatchewan River at Medicine Hat (AK001), to capture hydroclimatic variability at subbasin and basin scales, respectively. Calibration and verification statistics for the two regression models indicated skillful reconstructions of water year flow (Table 4). The models accounted for 37% and 43% of the instrumental variance and had significant skill when subjected to cross validation (Table 4). Regression residuals were normally distributed and behaved as a white noise process. The calibration models captured the low-frequency and low-flow variability well but underestimated high flows throughout the calibration period (Figure 3). Tree ring reconstructions typically underestimate high flows as other environmental conditions become limiting during wet years [*Fritts*, 1976]. This accounts for much of the unexplained variance. The low flows in the instrumental record during the 1930s were under represented by both models (Figure 3), but not to the extent that high flows are underestimated. Plotted with the full reconstructions of average water year flow (Figure 3) are 95% confidence levels based on the root-mean-square-error estimates from the verification period [*Jain et al.*, 2002], the calibration mean; the lowest 10th and highest 90th flow percentiles, and sample depth through time against the right *y* axis. A 25-year spline with a 50% frequency cutoff, the frequency at which 50% of the amplitude of signal is retained, highlights low-frequency variability in the reconstruction.

[21] Sustained wet and dry intervals were identified for each reconstruction using flows in the 75th and 25th percentiles, respectively. For the 387-year Oldman River record, the longest wet interval occurred from 1897 to 1913, the period when most Euro-Canadian settlers arrived in the region; and the longest dry interval was from 1862 to 1876, shortly prior to settlement. For the South Saskatchewan River, the longest wet interval was from 1825 to 1841 and longest dry interval was during 1552 to 1571. The SSR record extending to 1400 is characterized by low flows from the 1470s to the 1570s, with extreme drought in the 1560s (Table 5). Severe hydrological droughts, defined as flows in the lowest 10th percentile,

Table 3. Principal Components Analysis of Standard Chronologies From the Oldman River Subbasin for Two Common Periods Using the Covariance Matrix Method[a]

Common Period	Predictors	Extracted Principal Components[b]
1400–2004	CBC and OLR_1	604-PC1 (84.3) 604-PC2 (15.6)
1618–2004	BDC, BUC, CAC, CBC DUC, LBC, OLR_1, WSC	386-PC1 (77.7)

[a]Standard chronologies.
[b]Explained variance. Percentages are given in parentheses.

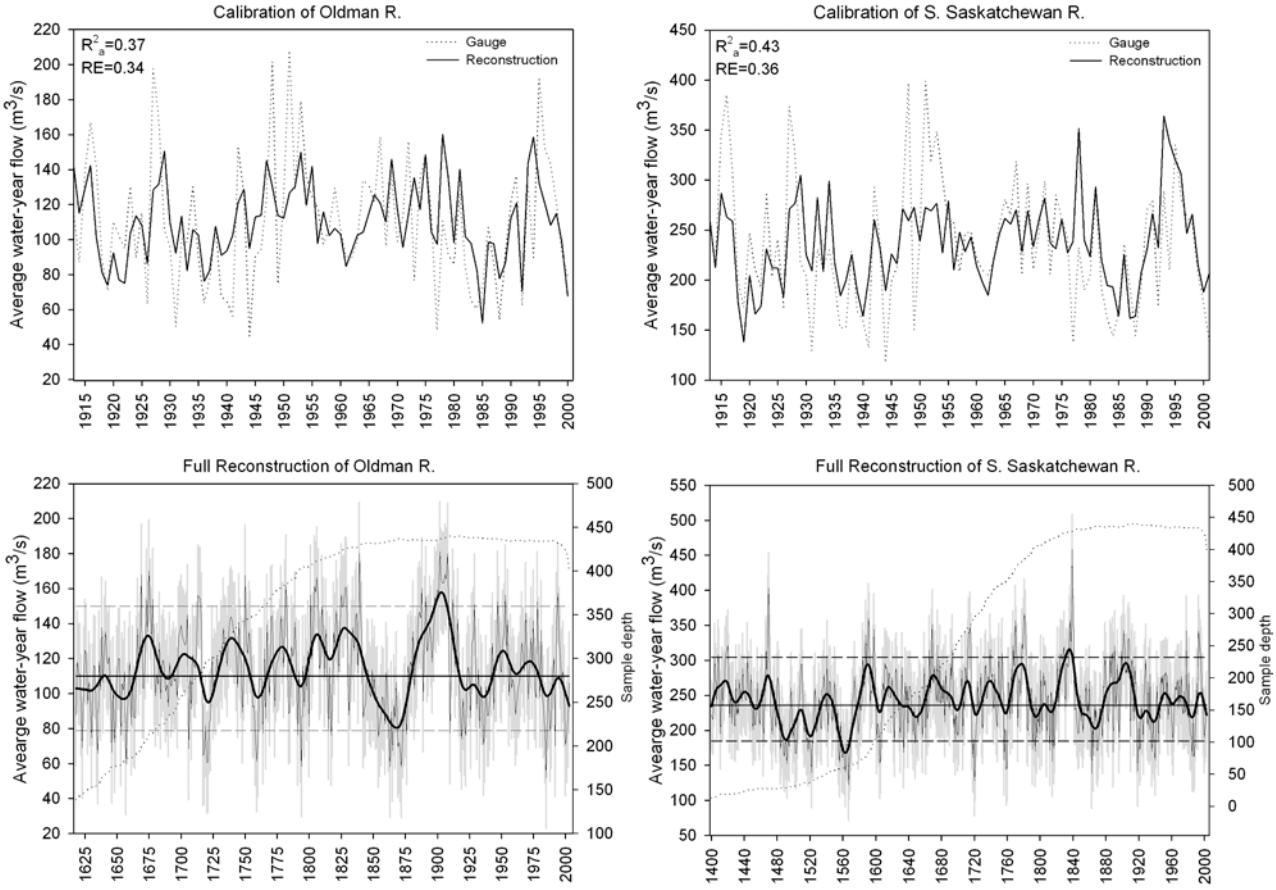

Figure 3. (top left) Oldman River and (top right) South Saskatchewan River gauge and reconstructed water year flows (previous October to current September) for the calibration period (1912–2001). (bottom) The full reconstruction (black lines) of water year flows for (left) the Oldman River for the period of 1618–2003 and (right) South Saskatchewan River for the period of 1400–2003; gray lines are the 95% confidence interval calculated from the root-mean-square error estimates from the verification period, the heavy black line is a 25-year spline with 50% frequency response, the solid horizontal line is the calibration mean, and dashed horizontal lines represent the 10th and 90th percentiles. Sample depth through time is plotted on the right-hand y axis.

were identified and the top ten worst droughts were compiled by reconstruction (Table 5). The earliest severe drought common to both reconstructions occurred from 1717 to 1721, when at least one of these years was ranked as one of the ten driest years. Another severe drought year common to both reconstructions was 1863, which ranked second and third for the Oldman and South Saskatchewan rivers, respectively. Both reconstructions had only one drought year in the postsettlement (instrumental) period; 1985 (first) and 1919 (sixth) in the Oldman River and SSR records, respectively (Table 5). Although the 1930s are considered one of the worst droughts periods in memory in western North America, it does not appear as an extreme drought in either reconstruction.

[22] The results of the single-spectrum MTM analysis (Figure 4) of the reconstructions show a highly significant multidecadal (~65 years) component of variability in both reconstructions together with significant variability at interannual time scales (2–6 years) in the El Niño-Southern Oscillation (ENSO) band. The results of the wavelet power spectrum mirror those of the MTM spectrum, but with the additional context of the time frequency domain. The significant multidecadal (~65 years) component is evident in the wavelet spectrum during sustained low flows in the 1500s for the South Saskatchewan reconstruction, corresponding to the "megadrought" identified in the western United States [*Stahle et al.*, 2000]; and during the 1800s in both reconstructions (Figure 4). Significant interannual variability is evident throughout the wavelet power spectrum for both reconstructions. Previous studies [e.g., *Shabbar and Skinner*, 2004; *Gobena and Gan*, 2006] identified significant modes of

Table 4. Regression Statistics of Tree Ring-Based Reconstructions of Streamflow

Gauge ID	Reconstruction Period	Predictors in Model	R^2	Adjusted R^2	RE	F Ratio	SE	$RMSE_v$
AD007	1618–2003	386-PC1, PEC, WCH	0.394	0.373	0.34	13.51	28.52	28.92
AK001	1400–2003	604-PC1, 604-PC2	0.443	0.430	0.36	22.51	47.93	50.35

Table 5. Top Ranked Extreme Dry Years for Both Reconstructions[a]

Rank	Oldman River	South Saskatchewan River
1	1985	1567
2	1863	1720
3	1872	1863
4	1794	1522
5	1657	1563
6	1720	1919
7	1721	1759
8	1759	1760
9	1717	1721
10	1718	1568

[a]Extreme dry years are <10th percentile.

interannual and interdecadal variability in the observed hydroclimate of western Canada, and associated sea surface temperature (SST) forcing, specifically the ENSO and Pacific Decadal Oscillation (PDO). While, our tree ring series have an interdecadal (~13 years) peak, the multidecadal component is stronger; a finding similar to previous tree ring studies [e.g., *Gedalof and Smith*, 2001; *Gray et al.*, 2003]. A difference in dominant modes between proxy and instrumental records could point to the limitation of the shorter records for capturing low-frequency signals and to the nonstationarity of SST forcing, whereby for example interdecadal variability may be recently more energetic.

6. Discussion

[23] Research in dendrohydrology has been characterized by the use of increasingly dense networks of moisture-sensitive tree ring chronologies for constructing proxy records of regional hydroclimate. For example, there has been a series of reconstructions of the paleohydrology of the Colorado River [*Stockton and Jacoby*, 1976; *Hidalgo et al.*, 2001; *Woodhouse et al.*, 2006; *Timilsena et al.*, 2007] as chronologies are added to the network of tree ring sites in the basin and new statistical methods are applied to tree ring and hydroclimatic data. By developing a network of new moisture-sensitive tree ring chronologies in the runoff-generating upper reaches of the South Saskatchewan River Basin (SSRB), we were able to produce the first reconstruction of the annual flow of the Oldman River and a second reconstruction of the annual flow of the South Saskatchewan River (SSR). The initial reconstruction for the SSR by *Case and MacDonald* [2003] (CM) was based on tree ring data from limber pine at only two sites in the SSRB that were both xeric. Our new network of 14 sites in

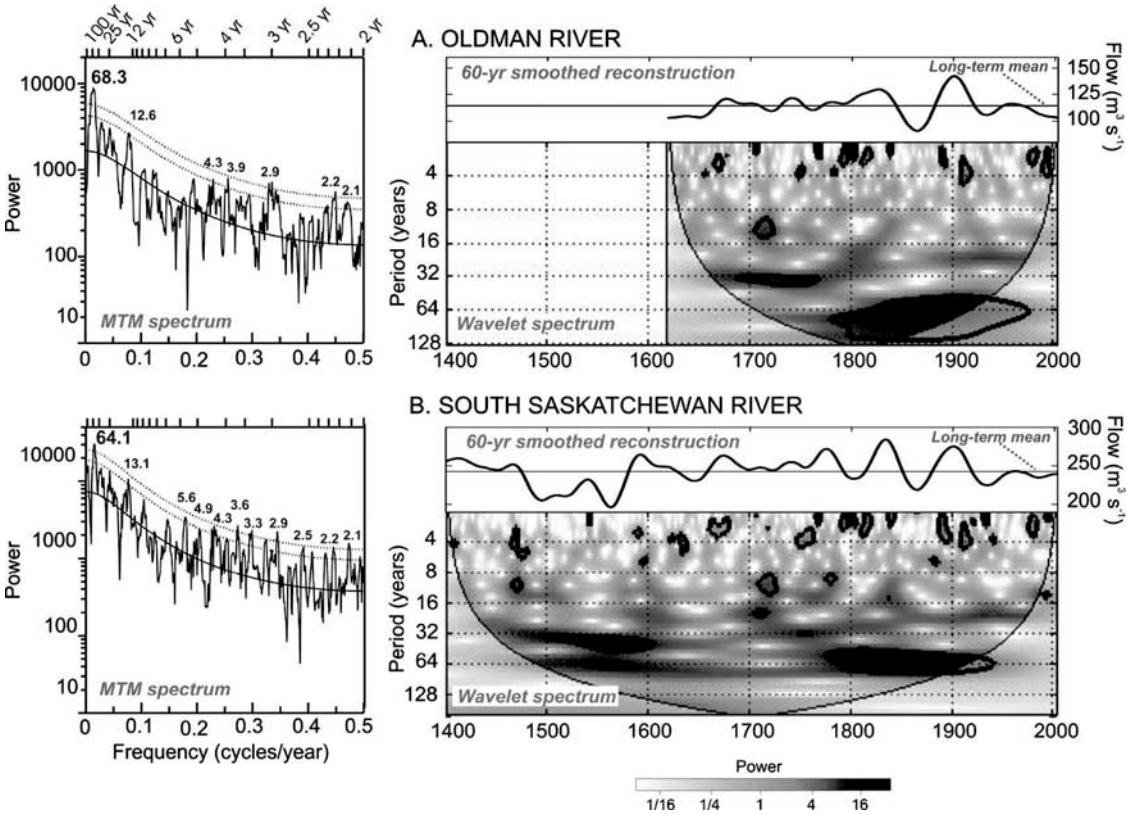

Figure 4. (left) The results of the single-spectrum MTM analysis showing a highly significant multidecadal (~65 years) component of variability in both reconstructions together with significant variability at interannual time scales (2–6 years). The dotted lines represent the median and 95 and 99% levels of significance. The significant spectral peaks are labeled. (right) The wavelet power spectrum and a 60-year low-pass-filtered version of the streamflow reconstructions for (a) Oldman River and (b) South Saskatchewan River show a prominent multidecadal mode of variability. In the wavelet plots, the thick black contour designates the 5% significance level against red noise, and a lighter shade is used to show the cone of influence where edge effects might be important.

the SSRB includes Douglas fir at 10 mesic sites and thus encompasses a range of local hydroclimatic conditions, including signals of late fall and midwinter precipitation. Our results are not directly comparable to *Case and MacDonald* [2003] because, in an attempt to produce more robust models and reconstructions, we used somewhat different methods to create, calibrate and validate the tree ring models of streamflow. These methods included PCA, enabled by dense sampling in the Oldman River basin, and various methods and statistics (e.g., expressed population signal, leave-*n*-out cross validation) to measure and express the validity and predictive capacity of the models. Foremost, we were able to achieve much more replication, a basic principle of dendrochonology, and thus a longer record for the SSR (605 years versus 522 years for CM) but more importantly much greater sample depth in the early years.

[24] Similarities between the CM reconstruction of the SSR and ours presented here reflect some common signals between the two sets of tree ring chronologies. Both reconstructions include 1717, 1718, 1720, 1721 and 1815 among the 10 worst drought years. In the CM record, however, severe droughts occurred mainly during the 18th and 19th centuries, while in our reconstructions severe droughts occurred mainly in the16th and 18th centuries in the South Saskatchewan River (Figure 3) and the 18th century in the Oldman River (Figure 3). The megadrought of the 16th century that extended from northwestern Canada [*Szeicz and MacDonald*, 1996] to Mexico [*Stahle et al.*, 2000] and the Atlantic Coast [*Stahle et al.*, 1998] was captured in our SSR reconstruction, where the period from 1552 to 1571 had the longest sustained low flow on record, and 3 years (1563, 1567 and 1568) ranked in the top 10 worst drought years (Table 5). Another sustained drought, from the 1850s to the early 1870s, is prominent in all reconstructions of streamflow [*Case and MacDonald*, 2003; *Bonin and Burn*, 2005; *Watson and Luckman*, 2005a; *Beriault and Sauchyn*, 2006] and precipitation [e.g., *Sauchyn et al.*, 2003; *Watson and Luckman*, 2005b] from the western interior and cordillera. It also appears in historical archives; specifically in the journals of the Palliser expedition that contained the infamous remark that the region corresponding to the SSRB "will forever be comparatively useless" [*Sauchyn et al.*, 2003, p. 163; *Rannie*, 2006].

[25] Our tree ring reconstructions of streamflow in the SSRB provide a long-term context for the gauge records that are basis for water supply planning in the watershed. The Prairie Provinces Master Agreement on Apportionment, governing interprovincial streamflows, was based on computed natural flows from 1912 to 1967 [*PPWB*, 1969], while allocations in Alberta are based on the computed natural flow from 1919 to 2001 [*Alberta Environment*, 2005]. There are approximately 200,000 water licenses and registrations in the SSRB, where irrigation accounts for 75% of water allocations, as compared to 0.99% for preserving aquatic environments. The Oldman River accounts for 87% of irrigation allocations and the volume allocated at times exceeds natural flow [*Alberta Environment*, 2005]. The nearly full allocation of surface water in the Oldman and Bow River basins has led to a moratorium on the granting of new surface water licenses [*Alberta Environment*, 2005]. This level of demand for the water resources of the SSRB suggests that an awareness of interannual to multidecadal variation in hydroclimate is essential for water resource management and planning in the basin. This study has clearly documental long-term low-frequency variability in regional hydroclimate that must be considered in any interpretation of recent trends in gauged streamflow and projections of future water supplies in the basin.

[26] The energy provider, Manitoba Hydro, uses the basin wide hydrological drought of 1937 to 1944 to represent the worst-case scenario for their operations on the basis of water supplies from the Saskatchewan-Nelson, Churchill, Red and Winnipeg River basins [*Girling*, 2006]. Placing this "worst-case scenario" in the context of our reconstruction, by expressing streamflow as a percentage difference from the full reconstruction mean, the 1937–1944 drought represents a 10% negative departure for the Oldman River and a 16% flow deficit for the South Saskatchewan River. If we apply the same analysis to the most severe drought in the reconstruction, 1717–1721, there was a 40% deficit for the Oldman River, and a 32% negative departure for the South Saskatchewan River. Thus, the most severe drought in the tree ring reconstruction represents flows that are roughly four times lower than the institutional worst-case scenario.

[27] A significant decreasing trend in the annual flow of the South Saskatchewan River is documented in recent analyses of gauge records [*Rood et al.*, 2005; *Schindler and Donahue*, 2006]. Much of this declining flow can be attributed to water storage, diversion and consumption but it is also consistent with projections of future flows derived by coupling hydrologic models and climate change scenarios [*Pietroniro et al.*, 2006]. This trend will level off at mean annual future flows according to changes in demand versus supply, where future raw water supplies will be determined by global warming impacts on the hydrology of the headwater basins and imposed on the interannual to multidecadal variability revealed in our tree ring reconstructions. The significant multidecadal ($\sim$65 year) mode of variability in our reconstructed flows of the Oldman and South Saskatchewan rivers suggest that trends inferred from decades-long instrumental records could represent low-frequency variability inherent in the regional hydroclimate.

7. Conclusion

[28] The objective of this research was to examine long-term hydroclimatic variability in the South Saskatchewan River Basin (SSRB) by deriving robust reconstructions of streamflow at two scales from a network of new tree ring chronologies in the major runoff producing subbasins. Average water year flow was reconstructed for gauges on the Oldman and South Saskatchewan rivers. The tree ring models accounted for 37% and 43% of the instrumental variance, respectively. These proxy streamflow records, extending to 1400, reveal the timing, duration and relative severity of sequences of high and low flows. Because much of the unexplained variance in the calibration period is the underestimation of high flows, we have more confidence in the interpretation of the low flows which consistently correspond to narrow tree rings, capturing the timing and duration of drought. While the 20th century is representative of drought frequency over the long term, there are droughts of greater severity and especially duration in the

proxy record. Thus the 605 years of reconstructed flow presented in this paper provide an important context for institutional worst-case scenarios which rely on instrumental records that are generally shorter than the significant low-frequency variability captured by our tree ring records. In particular, the significant interdecadal variability in our tree ring reconstructions of streamflow provide an alternative interpretation of trends in gauge records that are decades in length.

[29] Despite the amount of new tree ring data and processing that we applied to skilful reconstructions of streamflow in the SSRB, tree ring width indices still account for less than 50% of the variance in the gauge records. In snow dominated basins, spring snowmelt and precipitation in the cooler months are the major contributors to streamflow. Soil moisture recharged from winter precipitation is available for use by trees at the beginning of the growing season, and biological processes important for the overall water and energy balances of the trees are not restricted to cambial growing season but continue year round [*Fritts*, 1976; *Meko et al.*, 1995]. Thus to some extent, our tree ring records have a snowmelt signal; there are significant correlations with February precipitation at some sites and with spring soil water availability at most sites. However, despite developing a new network of tree ring chronologies in the upper reaches of the SSRB to capture a wider range of local hydroclimate conditions, the underestimation of high annual flows persists. Therefore this study also has verified that tree growth at lower elevations does not capture the full magnitude of snowmelt infiltration and runoff despite some correlation between tree ring and winter precipitation data. Adding higher-elevation snowpack sensitive tree ring chronologies to the pool of predictors of streamflow [*Watson and Luckman*, 2006] should produce models that account for a larger percentage of the variance in the instrumental records.

[30] **Acknowledgments.** This research was funded by NSERC, Manitoba Hydro and the Inter-American Institute for Global Change Research. For assistance in the field and lab, we thank Antoine Beriault, Laura Pfiefer and Melissa Ranalli. Special thanks go to Dave Meko (University of Arizona) and the Prairie Adaptation Research Collaborative. We also thank three anonymous reviewers whose thoughtful comments and suggestions resulted in an improved manuscript.

References

Alberta Environment (1998), South Saskatchewan River Basin historical natural flows 1912 to 1995, 181 pp., Edmonton, Alberta, Canada.

Alberta Environment (2002), South Saskatchewan River sub-basin contributions to international and interprovincial water-sharing agreements, *Publ. 703*, 39 pp., Edmonton, Alberta, Canada.

Alberta Environment (2005), South Saskatchewan River Basin water allocation, 39 pp., Edmonton, Alberta, Canada.

Barnett, T. P., J. C. Adam, and D. P. Lettenmaier (2005), Potential impacts of warming climate on water availability in snow-dominated regions, *Nature*, *438*, 303–309, doi:10.1038/nature04141.

Beriault, A. L., and D. J. Sauchyn (2006), Tree-ring reconstructions of streamflow in the Churchill River Basin, northern Saskatchewan, *Can. Water Resour. Assoc. J.*, *31*, 249–262.

Bonin, D. V., and D. H. Burn (2005), Use of tree ring reconstructed streamflows to assess drought, *Can. J. Civ. Eng.*, *32*, 1114–1123, doi:10.1139/l05-069.

Briffa, K. R., and P. D. Jones (1990), Tree-ring standardization and growth-trend estimation, in *Methods of Dendrochronology: Applications in the Environmental Sciences*, edited by E. R. Cook and L. A. Kairiukstis, pp. 137–152, Kluwer Acad., Dordrecht, Netherlands.

Brubaker, K. L., and A. Rango (1996), Response of snowmelt hydrology to climate change, *Water Air Soil Pollut.*, *90*, 335–343, doi:10.1007/BF00619293.

Case, R. A., and G. M. MacDonald (2003), Tree ring reconstructions of streamflow for three Canadian prairie rivers, *J. Am. Water Resour. Assoc.*, *39*, 703–716, doi:10.1111/j.1752-1688.2003.tb03686.x.

Cleaveland, M. K., and D. W. Stahle (1989), Tree-ring analysis of surplus and deficit run-off in the White River, Arkansas, *Water Resour. Res.*, *25*(6), 1391–1401, doi:10.1029/WR025i006p01391.

Cook, E. R. (1985), A time series approach to tree-ring standardization, Ph.D. dissertation, Univ. of Ariz., Tucson.

Cook, E. R., K. Briffa, S. Shiyatov, and V. Mazepa (1990), Tree-ring standardization and growth-trend estimation, in *Methods of Dendrochronology: Applications in the Environmental Sciences*, edited by E. R. Cook and L. A. Kairiukstis, pp. 104–123, Kluwer Acad., Dordrecht, Netherlands.

Fritts, H. C. (1976), *Tree Rings and Climate*, Academic, London.

Fritts, H. C., J. Guiot, and G. A. Gordon (1990), Tree-ring standardization and growth-trend estimation, in *Methods of Dendrochronology: Applications in the Environmental Sciences*, edited by E. R. Cook and L. A. Kairiukstis, pp. 178–185, Kluwer Acad., Dordrecht, Netherlands.

Gedalof, Z., and D. J. Smith (2001), Interdecadal climate variability and regime scale shifts in Pacific North America, *Geophys. Res. Lett.*, *28*, 1515–1518, doi:10.1029/2000GL011779.

Gedalof, Z., D. L. Peterson, and N. J. Mantua (2004), Columbia River flow and drought since 1750, *J. Am. Water Resour. Assoc.*, *40*, 1579–1592, doi:10.1111/j.1752-1688.2004.tb01607.x.

Ghil, M., et al. (2002), Advanced spectral methods for climatic time series, *Rev. Geophys.*, *40*(1), 1003, doi:10.1029/2000RG000092.

Girling, W. (2006), Manitoba hydro climate change impact and adaptation activities, paper presented at Hydropower and Climate Change Workshop, Can. Clim. Impacts and Adapt. Res. Network, Winnipeg, Manitoba, Canada, 2-3 March. (Available at http://c-ciarn.mcgill.ca/Bill%20Girling%20HP2006.pdf).

Gobena, A. K., and T. Y. Gan (2006), Low-frequency variability in southwestern Canadian stream flow: Links with large-scale climate anomalies, *Int. J. Climatol.*, *26*, 1843–1869, doi:10.1002/joc.1336.

Gray, S. T., J. L. Betancourt, C. L. Fastie, and S. T. Jackson (2003), Patterns and sources of multidecadal oscillations in drought-sensitive tree-ring records from the central and southern Rocky Mountains, *Geophys. Res. Lett.*, *30*(6), 1316, doi:10.1029/2002GL016154.

Grinsted, A., J. C. Moore, and S. Jevrejeva (2004), Application of the cross wavelet transform and wavelet coherence to geophysical time series, *Nonlinear Processes Geophys.*, *11*, 561–566.

Haan, C. T. (2002), *Statistical Methods in Hydrology*, 2nd ed., Iowa State Univ. Press, Ames, Iowa.

Hauer, R. F., J. S. Baron, D. H. Campbell, K. D. Fausch, S. W. Hostetler, G. H. Leavesley, P. R. Leavitt, D. M. McKnight, and J. A. Stanford (1997), Assessment of climate change and freshwater ecosystems of the Rocky Mountains, USA and Canada, *Hydrol. Processes*, *11*, 903–924, doi:10.1002/(SICI)1099-1085(19970630)11:8<903::AID-HYP511>3.0.CO;2-7.

Hidalgo, H. G., J. A. Dracup, G. M. MacDonald, and J. A. King (2001), Comparison of tree species sensitivity to high and low extreme hydroclimatic events, *Phys. Geogr.*, *22*(2), 115–134.

Holmes, R. (1983), Computer-assisted quality control in tree-ring dating and measurement, *Tree Ring Bull.*, *44*, 69–75.

Hughes, M. K., P. M. Kelly, J. R. Pilcher, and V. C. Lamarche Jr. (Eds.) (1982), *Climate From Tree Rings*, Cambridge Univ. Press, Cambridge, U. K.

Jain, S., C. A. Woodhouse, and M. P. Hoerling (2002), Multidecadal streamflow regimes in the interior western United States: Implications for the vulnerability of water resources, *Geophys. Res. Lett.*, *29*(21), 2036, doi:10.1029/2001GL014278.

Loaiciga, H. A., L. Haston, and J. Michaelsen (1993), Dendrohydrology and long-term hydrologic phenomena, *Rev. Geophys.*, *31*(2), 151–171, doi:10.1029/93RG00056.

Longley, R. W. (1953), Variability of annual precipitation in Canada, *Mon. Weather Rev.*, *81*, 131–134, doi:10.1175/1520-0493(1953)081<0131:VOAPIC>2.0.CO;2.

Mann, M. E., and J. M. Lees (1996), Robust estimation of background noise and signal detection in climatic time series, *Clim. Change*, *33*, 409–445, doi:10.1007/BF00142586.

Marshall, I. B., and P. H. Schut (1999), A national ecological framework for Canada-Overview, Ecosyst. Sci. Dir., Environ. Can., Ottawa.

McKay, G. A., R. B. Godwin, and J. Maybank (1989), Drought and hydrological drought research in Canada: An evaluation of the state of the art, *Can. Water Resour. J.*, *14*, 71–84.

Meko, D. (2006), Tree-ring inferences on water-level fluctuations of Lake Athabasca, *Can. Water Resour. J.*, *31*, 229–248.

Meko, D., M. Hughes, and C. W. Stockton (1991), Climate change and climate variability: The paleo record, in *Managing Water Resources Under Conditions of Climate Uncertainty, Proceedings of a Colloquium, Scottsdale, Arizona*, edited by Comm. on Clim. Uncertainty and Water Resour. Manage., pp. 71–100, Natl. Acad. Press, Washington, D. C.

Meko, D., C. W. Stockton, and W. R. Boggess (1995), The tree-ring record of severe sustained drought, *Water Resour. Bull.*, *31*(5), 789–801.

Michels, A., K. R. Laird, S. E. Wilson, D. Thomson, P. R. Leavitt, R. J. Oglesby, and B. F. Cumming (2007), Multi-decadal to millennial-scale shifts in drought conditions on the Canadian Prairies over the past six millennia: Implications for future drought assessment, *Global Change Biol.*, *13*(7), 1295–1307.

Nijssen, B., G. M. O'Donnell, A. F. Hamlet, and D. P. Lettenmaier (2001), Hydrologic sensitivity of global rivers to climate change, *Clim. Change*, *50*, 143–175, doi:10.1023/A:1010616428763.

Ostrom, C. W., Jr. (1990), *Time Series Analysis: Regression Techniques*, *Quant. Appl. Soc. Sci.*, vol. 07-009, 2nd ed.Sage, Newbury Park, Calif.

Pietroniro, A., B. Toth, and J. Toyra (2006), Water availability in the South Saskatchewan River Basin under climate change, paper presented at Climate Change and Water in the Prairies Conference, Univ. of Sask., Saskatoon, Canada, 21–23 June.

Prairie Provinces Water Board (PPWB) (1962), The effect of a change in vegetation on the runoff characteristics of Alberta streams, *Rep. 38*, 91 pp., Regina, Sask., Canada.

Prairie Provinces Water Board (PPWB) (1969), The 1969 master agreement on apportionment, Regina, Sask., Canada.

Rannie, W. F. (2006), A comparison of the 1858–59 and 2000–01 drought patterns on the Canadian Prairies, *Can. Water Resour. J.*, *31*, 263–274.

Rood, S. B., G. M. Samuelson, J. K. Weber, and K. A. Wywrot (2005), Twentieth-century decline in streamflows from the hydrographic apex of North America, *J. Hydrol.*, *306*(1–4), 215–233, doi:10.1016/j.jhydrol.2004.09.010.

Sauchyn, D. J., and S. Kulshreshtha (2008), The Prairies, in *From Impacts to Adaptation: Canada in a Changing Climate 2007*, edited by D. S. Lemmen et al., chap. 7, pp. 275–328, Gov. of Can., Ottawa.

Sauchyn, D. J., J. Stroich, and A. Beriault (2003), A paleoclimatic context for the drought of 1999–2001 in the northern Great Plains of North America, *Geogr. J.*, *169*(2), 158–167, doi:10.1111/1475-4959.05003.

Sauchyn, D. J., A. Pietroniro, and M. Demuth (2009), Upland watershed management and global change-Canada's Rocky Mountains and Western Plains, in *Mountains, Valleys and Flood Plains: Managing Water Resources in a Time of Global Change*, edited by A. Garrido and A. Dinar, chap. 3, pp. 32–49, Routledge, London.

Schindler, D. W., and W. F. Donahue (2006), An impending water crisis in Canada's western prairie provinces, *Proc. Natl. Acad. Sci. U. S. A.*, *103*, 7210–7216.

Schulman, E. (1945), Tree-rings and run-off in the south Platte River basin, *Tree Ring Bulletin*, *11*(3), 18–24.

Shabbar, A., and W. Skinner (2004), Summer drought patterns in Canada and the relationship to global sea surface temperatures, *J. Clim.*, *17*, 2866–2880, doi:10.1175/1520-0442(2004)017<2866:SDPICA>2.0.CO;2.

Smith, L. P., and C. W. Stockton (1981), Reconstructed streamflow for the Salt and Verde rivers from tree-ring data, *Water Resour. Bull.*, *17*(6), 939–947.

Stahle, D. W., M. K. Cleaveland, D. B. Blanton, M. D. Therell, and D. A. Gay (1998), The lost colony and Jamestown droughts, *Science*, *280*, 564–567, doi:10.1126/science.280.5363.564.

Stahle, D. W., E. R. Cook, M. K. Cleaveland, M. D. Therrell, D. M. Meko, H. D. Grissino-Mayer, E. Watson, and B. H. Luckman (2000), Tree-ring data document 16th century megadrought over North America, *Eos Trans. AGU*, *81*(12), 121, doi:10.1029/00EO00076.

St. George, S., and E. Nielsen (2002a), Flood ring evidence and its application to paleoflood hydrology of the Red River and the Assiniboine River in Manitoba, *Geogr. Phys. Quat.*, *56*(2–3), 181–190.

St. George, S., and E. Nielsen (2002b), Hydroclimatic change in southern Manitoba since A. D. 1409 inferred from tree rings, *Quat. Res.*, *58*, 103–111, doi:10.1006/qres.2002.2343.

St. George, S., and D. J. Sauchyn (2006), Paleoenvironmental perspectives on drought in western Canada, *Can. Water Resour. J.*, *31*, 197–204.

Stockton, C. W., and H. C. Fritts (1973), Long-term reconstruction of water level changes for Lake Athabasca by analysis of tree-rings, *Water Resour. Bull.*, *9*(5), 1006–1027.

Stockton, C. W., and G. C. Jacoby Jr. (1976), Long-term surface-water supply and streamflow trends in the Upper Colorado River Basin based on tree-ring analysis, *Lake Powell Res. Proj. Bull. 18*, 49 pp., Inst. of Geophys. and Planet. Phys., Univ. of Calif., Los Angeles.

Stokes, M. A., and T. L. Smiley (1968), *An Introduction to Tree-Ring Dating*, Univ. of Chicago Press, Chicago, Ill.

Szeicz, J. M., and G. M. MacDonald (1996), A 930-year ring-width chronology from moisture-sensitive white spruce (*Picea glauca* Moench) in northwestern Canada, *Holocene*, *6*, 345–351, doi:10.1177/095968369600600309.

Timilsena, J., T. C. Piechota, H. Hidalgo, and G. Tootle (2007), Five hundred years of hydrological drought in the upper Colorado River basin, *J. Am. Water Resour. Assoc.*, *43*(3), 798–812, doi:10.1111/j.1752-1688.2007.00064.x.

Watson, E., and B. H. Luckman (2005a), An exploration of the controls of pre-instrumental streamflow using multiple tree-ring proxies, *Dendrochronologia*, *22*, 225–234, doi:10.1016/j.dendro.2005.05.006.

Watson, E., and B. H. Luckman (2005b), Spatial patterns of pre-instrumental moisture variability in the southern Canadian Cordillera, *J. Clim.*, *18*, 2847–2863, doi:10.1175/JCLI3416.1.

Watson, E., and B. H. Luckman (2006), Long hydroclimate records from tree-rings in western Canada: Potential, problems and prospects, *Can. Water Resour. Assoc. J.*, *31*(4), 205–228.

Wheaton, E. E., L. M. Arthur, B. Chorney, S. Shewchuk, J. Thorpe, J. Whiting, and V. Wittrock (1992), The Prairie drought of 1988, *Clim. Bull.*, *26*, 188–205.

Wheaton, E. E., S. Kulshreshtha, and V. Wittrock (Eds.) (2005), *Canadian droughts of 2001 and 2002: Climatology, impacts and adaptations*, *Publ. 11602-1E03*, 1323 pp., Agric. and Agri Food Can., Ottawa.

Wigley, T. M., K. R. Briffa, and P. D. Jones (1984), On the average value of correlated time series, with application in dendroclimatology and hydrometeorology, *J. Clim. Appl. Meteorol.*, *23*, 201–213, doi:10.1175/1520-0450(1984)023<0201:OTAVOC>2.0.CO;2.

Woodhouse, C. A. (2001), Tree-ring reconstruction of streamflow for the Colorado Front Range, *J. Am. Water Resour. Assoc.*, *37*(3), 561–569, doi:10.1111/j.1752-1688.2001.tb05493.x.

Woodhouse, C. A., S. T. Gray, and D. M. Meko (2006), Updated streamflow reconstructions for the Upper Colorado River Basin, *Water Resour. Res.*, *42*, W05415, doi:10.1029/2005WR004455.

J. N. Axelson, Pacific Forestry Centre, Canadian Forest Service, Natural Resources Canada, 506 West Burnside Road, Victoria, BC V8Z 1M5, Canada.

J. Barichivich, Climatic Research Unit, University of East Anglia, Norwich NR4 7TJ, UK.

D. J. Sauchyn, Prairie Adaptation Research Collaborative, University of Regina, Regina, SK S4S 7J7, Canada. (sauchyn@uregina.ca)

Northern Rocky Mountain streamflow records: Global warming trends, human impacts or natural variability?

Jeannine-Marie St. Jacques,[1] David J. Sauchyn,[1] and Yang Zhao[2]

Received 4 December 2009; revised 11 February 2009; accepted 18 February 2009; published 26 March 2010.

[1] The ~60 year Pacific Decadal Oscillation (PDO) is a major factor controlling streamflow in the northern Rocky Mountains, causing dryness during its positive phase, and wetness during its negative phase. If the PDO's influence is not incorporated into a trend analysis of streamflows, it can produce detected declines that are actually artifacts of this low-frequency variability. Further difficulties arise from the short length and discontinuity of most gauge records, human impacts, and residual autocorrelation. We analyze southern Alberta and environs instrumental streamflow data, using void-filled datasets from unregulated and regulated gauges and naturalized records, and Generalized Least Squares regression to explicitly model the impacts of the PDO and other climate oscillations. We conclude that streamflows are declining at most gauges due to hydroclimatic changes (probably from global warming) and severe human impacts, which are of the same order of magnitude as the hydroclimate changes, if not greater. **Citation:** St. Jacques, J.-M., D. J. Sauchyn, and Y. Zhao (2010), Northern Rocky Mountain streamflow records: Global warming trends, human impacts or natural variability?, *Geophys. Res. Lett.*, *37*, L06407, doi:10.1029/2009GL042045.

1. Introduction

[2] Under anthropogenic global warming scenarios, southern Alberta, Canada, is projected to see decreased streamflow, and northern Alberta increased streamflow in the next century (see *Intergovernmental Panel on Climate Change* (*IPCC*) [2007, Figure 10.12] for multi-model mean run-off changes). Detection of any developing trends in the observed instrumental streamflow records is complicated by the fact that the Alberta hydroclimate, like that of much of northwestern North America, displays strong periodic cycles linked to the low-frequency Pacific Decadal Oscillation (PDO) [*Mantua et al.*, 1997; *Stewart et al.*, 2005]. The PDO is a pattern of climate variability that shifts phases on an inter-decadal time scale, usually at about 20 to 35 years [*Minobe*, 1997; *Mantua and Hare*, 2002]. In 1890, the PDO entered into a predominately cool (negative) phase, which continued until 1925 when a warm (positive) phase began. In 1947, the PDO shifted back into a cool phase, which lasted until 1977, whereupon a warm phase began. Winter precipitation in Alberta is higher when the PDO is in a negative phase [*Mantua et al.*, 1997; *Comeau et al.*, 2009]. A strong negative relationship exists between the PDO and streamflow in south and central Alberta, while a weak positive relationship exists in northwestern Alberta (Figure 1). Therefore, south and central Alberta are wetter when the PDO is in its negative phase and drier when the PDO is positive.

[3] The ~60 year low frequency cycle of the PDO [*Minobe*, 1997] can potentially generate a declining linear trend in short instrumental streamflow records. Like much of the western North American high-density hydrological monitoring network, many Alberta instrumental streamflow records begin in the 1950s (a period of strongly negative PDO, hence high Alberta streamflow), or omit the 1930s and early 1940s (periods of high positive PDO, hence low Alberta streamflow). If the influence of the PDO (i.e., high flows 1947–1976, low flows 1977–2007) is not taken into account in an analysis of northwestern North American instrumental hydroclimatic records, declines could be detected and linked to global warming, while they are actually artifacts of the sampling period and the PDO phase changes [e.g., *Chen and Grasby*, 2009].

[4] There are additional difficulties with using the instrumental records to reach a conclusion of declining surface water supplies in the northern Rocky Mountains. These records are short, typically having periods of record of ~40–50 years in northern Alberta and ~95 years in southern Alberta. They are frequently discontinuous with gaps, especially in the 1930s (due to economic collapse) and the 1940s (due to war). Heavy human impact from water consumption, diversion and storage, especially in southern Alberta, obscures the natural hydrology. Less obvious, but very serious statistically, is the frequent autocorrelation in the fitted residuals from regression using hydrometric data, which results in the overestimation of the effective sample size [*Zheng et al.*, 1997]. Therefore, classical linear regression and Mann-Kendall non-parametric methods can disproportionately reject a null hypothesis of no trend [*Zheng et al.*, 1997; *Zhang et al.*, 2001; *Burn and Hag Elnur*, 2002; *Yue et al.*, 2002]. In this paper, we examine instrumental streamflow records from the northern Rocky Mountains for trends, while addressing these important issues.

2. Statistical Methodology

[5] We analyzed instrumental streamflow records from southern Alberta and environs to determine if significant trends existed which could be attributable to global warming, while explicitly including the possible effects of the PDO and other interannual regional circulation anomalies to account for hydroclimatic variability. Low-frequency variability (i.e., slightly smoothed data) was analyzed given the associated severe socio-economic and ecological impacts of prolonged drought. High-frequency variability in precipitation and streamflow can be accommodated via conventional hazard

[1]Prairie Adaptation Research Collaborative, University of Regina, Regina, Saskatchewan, Canada.
[2]Department of Mathematics and Statistics, University of Regina, Regina, Saskatchewan, Canada.

0094-8276/10/2009GL042045

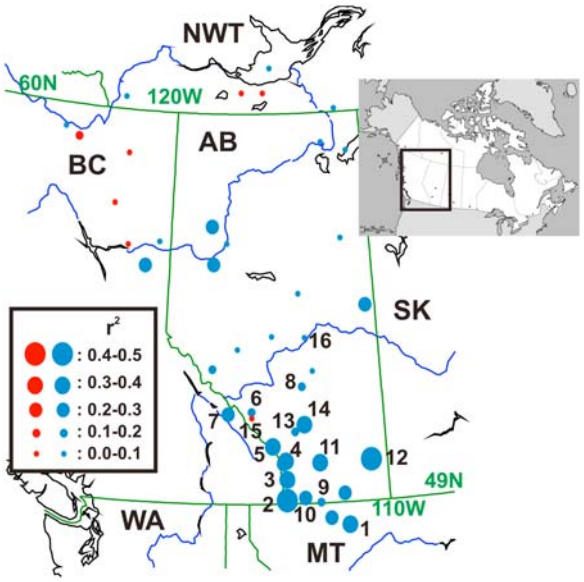

Figure 1. Pearson's correlation coefficients between Alberta and environs mean daily streamflows and the November–March Pacific Decadal Oscillation index (PDO) of the same year. Both streamflows and PDO were smoothed by a 5-year binomial filter. Gauges used were those with the longest continuous records. Dark red (light blue) circles denote positive (negative) correlation. Numbers denote the gauge locations of Table 1 (for regulated flows, the actual flow record and the naturalized record have the same gauge location).

mitigation strategies (insurance, reservoir storage, etc.), but not low frequency variability (i.e., sustained drought), which is a much more challenging climate hazard. Furthermore, if a trend were absent in the low-pass filtered data, it would be absent in the original data, as the particular filter used, a binomial smoother of five years, passes a linear trend without distortion [*Brockwell and Davis*, 2002].

[6] The above problems with streamflow data were addressed as follows: We extracted the longest and most complete streamflow records for southern Alberta and its near environs from the Water Survey of Canada (HYDAT) (http://www.wsc.ec.gc.ca/) and the National Water Information System (http://waterdata.usgs.gov/nwis/sw) databases. In addition to gauge records from unregulated streams, a streamflow database produced by Alberta Environment provided naturalized daily flows and void-filled records to overcome the effects of human impacts and gaps in the time series [*Seneka*, 2004]. Mean daily flows averaged over the year were used, because annual averaging normalizes the data by the Central Limit Theorem [*Wilks*, 2006], which allowed the use of more powerful parametric statistics. Shapiro-Wilks tests confirmed that most records were normally distributed, and that departures from normality were mild, except in two cases: the observed flows of the Spray and Red Deer Rivers.

[7] Generalized Least Squares (GLS) computes time series regression with serially correlated residuals and is therefore suitable for hydrological data [*Brockwell and Davis*, 2002]. Autoregressive-moving-average (ARMA(p,q)) models were fit to the residuals using a Maximum Likelihood Estimator. Open-source software from the R statistical programming language was used (http://www.r-project.org/).

[8] If there is a significant response of Alberta streamflow to any atmospheric-oceanic circulation anomaly at inter-annual to multi-decadal scales, and this response is not modeled, the ratio of trend signal to noise is reduced and a real trend, if present, may not be detectable. However, where the internal forcing can be represented by a linear response to some explanatory variable (e.g., the PDO), the variable can be included in the model to reduce the noise level and improve the detection of any existing trend [*Zheng et al.*, 1997; *Zheng and Basher*, 1999]. Also, if the PDO is not included in the model, its effect on precipitation and runoff can be mistaken for a linear trend extending over several decades. We also explored the influence of the North Atlantic Oscillation (NAO), as a proxy for the short-duration Arctic Oscillation record, and the El Nino-Southern Oscillation (ENSO). The climate indices used are the winter averaged (November–March) PDO, the winter averaged (December–March) NAO, and the annually averaged Southern Oscillation Index (SOI), obtained from Earth Systems Research Laboratory (National Oceanic and Atmospheric Administration, 2009, http://www.cdc.noaa.gov/ClimateIndices/). A linear trend and the PDO, NAO and SOI were included as predictors in the GLS regression models. Since streamflow is naturally lagged and smoothed from precipitation by surface and subsurface hydrology, and large-scale climatic phenomena act most prominently at inter-annual time scales, the stream observations were lagged relative to the climate indices by 0, ±1, and +2 years, and a binomial smoother of five years was applied to both the stream and climate data. The climate indices and their lags showed only minor collinearity.

[9] Sixteen stream gauges in southern Alberta and its environs were chosen for analysis based on the length and completeness of the records and natural flow regimes [*Alberta Environmental Protection*, 1998] (Table 1, and auxiliary material Figure S1 and Table S1).[1] Eight of the gauges are on unregulated or slightly regulated river runs. Eight of the gauges measure regulated flows and in these cases, the observed actual flows and the reconstructed naturalized flows compiled by Alberta Environment were separately analyzed, providing an additional 16 records. Fourteen of the gauges are located in Alberta, one in adjacent Montana, and one nearby in British Columbia. Most records (21 out of 24) span at least 90 years.

[10] The statistical model used in this study is

$$Q_t = \mu + \lambda T_t + \beta_1 x_{1,t} + \ldots + \beta_k x_{k,t} + \varepsilon_t, t = 1, \ldots, L, \quad (1)$$

where $\{Q_t\}$ is mean daily streamflow for year t, index t runs over L years; μ is the mean streamflow over all L of these years; T_t is a linear trend with coefficient λ representing the trend to be detected; $\{x_{i,t}, t = 1, \ldots, L\}$ is the i^{th} explanatory variable; k is the number of explanatory variables; β_i is the coefficient for the i^{th} explanatory variable; and $\{\varepsilon_t\}$ is the residual time series, which is an autoregressive-moving average process of order (p,q) [ARMA(p,q)]. An optimum minimal subset of significant predictors and an optimum

[1] Auxiliary materials are available in the HTML. doi:10.1029/2009GL042045.

Table 1. Trends in Southern Alberta and Environs Streamflows[a]

Flow Record	Actual flow record			Naturalized flow record			Human impact/yr
	Record period	Significant linear trend?	Change %/yr	Record period	Significant linear trend?	Change %/yr	
1. Marias R. near Shelby, MT	1912–2007	**decreasing**	**−0.26**	n.a.	n.a.	n.a.	n.a.
2. Waterton R. near Waterton Park	1912–2007	none	−0.05	n.a.	n.a.	n.a.	n.a.
3. Castle R. near Beaver Mines	1945–2007	none	−0.04	n.a.	n.a.	n.a.	n.a.
4. Oldman R. near Waldron's Corner	1950–2007	**increasing**	**0.43**	n.a.	n.a.	n.a.	n.a.
5. Highwood R. at Diebel's Ranch	1952–2007	none	0.11	n.a.	n.a.	n.a.	n.a.
6. Bow R. at Banff	1911–2007	**decreasing**	**−0.12**	n.a.	n.a.	n.a.	n.a.
7. Columbia R. at Nicholson, BC	1917–2007	none	−0.001	n.a.	n.a.	n.a.	n.a.
8. Red Deer R. at Red Deer	1912–2007	**decreasing**	**−0.22**	n.a.	n.a.	n.a.	n.a.
9. St. Mary R. at International Boundary	1903–2007	**decreasing**	**−0.46**	1912–2001	none	0.006	−0.47
10. Belly R. near Mountain View	1912–2007	none	0.02	1912–2001	none	0.02	−0.002
11. Oldman R. near Lethbridge	1912–2007	**decreasing**	**−0.76**	1912–2001	**decreasing**	**−0.18**	−0.58
12. S. Saskatchewan R. at Medicine Hat	1912–2007	**decreasing**	**−0.36**	1912–2001	**increasing**	**0.05**	−0.41
13. Elbow R. below Glenmore Dam	1911–2007	**decreasing**	**−0.70**	1912–2001	**decreasing**	**−0.34**	−0.36
14. Bow R. at Calgary	1912–2007	**decreasing**	**−0.16**	1912–2001	**decreasing**	**−0.16**	−0.01
15. Spray R. at Banff	1911–2007	**decreasing**	**−2.20**	1912–2001	**decreasing**	**−0.11**	−2.09
16. N. Saskatchewan R. at Edmonton	1912–2007	**decreasing**	**−0.14**	1911–2007	**decreasing**	**−0.10**	−0.04

[a]The first eight records are from unregulated rivers, therefore only the actual flow records exist. The last eight rivers are regulated and both actual flow and naturalized flow records exist, giving a further 16 records. Change%/yr calculated as 100x trend line slope/mean daily flow averaged over record period (bold denotes significant). Human impact/yr is the difference between the Change%/yr of the actual and the corresponding naturalized flows.

minimal ARMA(p,q) residual model were chosen using the corrected Akaike Information Criterion (AIC_c) goodness-of-fit statistic [*Brockwell and Davis*, 2002] applied to all predictor subsets of size ≤ 6, and for all $p \leq 8$ and $q \leq 5$. Simulation results by *Hurvich and Tsai* [1989] suggested that the AIC_c outperforms many other model selection criteria, including the AIC and the BIC, when the number of total estimated parameters is more than 10% of the sample size.

[11] The non-zero significance of the trend coefficient λ was tested by the Neyman-Pearson statistic (RP) [*Zheng et al.*, 1997] using the null model of the optimum set of explanatory variables (minus the trend variable if included in the optimum set; Table 1) versus the alternative model of the optimum set of explanatory variables together with the linear trend (if not already added). The RP is asymptotically distributed as a chi-square distribution with one degree of freedom. If the estimated RP is greater than the 0.10 percentile of $\chi^2_{(1)}$, the trend is significant at the 90% level. To assess rates of change, trend lines were calculated based upon the fitted multiple regressions with the climate indices set to zero (i.e., $Q_t = \mu + \lambda T_t$). The rate of change per year (Change%/yr) was expressed as a percentage of the mean daily flow, averaged over the entire period of record (i.e., $100\lambda/mean(Q_t)$) [*Rood et al.*, 2005]. Human impact could be estimated as the difference between the Change%/yr of the actual and the corresponding naturalized flows.

3. Results and Discussion

[12] Surface water supplies are indeed becoming scarcer in southern Alberta even when the confounding effects of the PDO and other sources of natural variability are factored out. We found fifteen significant decreasing linear trends in the streamflow records, versus only two increasing linear trends and seven null trends (Figure 2a, Table 1 and Table S1). There were no strong differences between the eight unregulated headwater gauges with three detected declining trends, and the eight naturalized flow records (at downstream gauges), five with declining trends, although the number of available long records is limited. There was a geographical pattern, with the gauges in the Bow River watershed more likely to show declining flow.

[13] The current year PDO or a lead or lag was the explanatory variable that appeared most consistently in the optimum predictor set, with only two exceptions: the actual flows of the Elbow and Spray Rivers (Figure 2b and Table S1). The PDO's strong influence was also shown by box plots of the individual stream records divided into the four phases of the PDO over the past century: higher flows in the cold phases (1900–1924 and 1946–1976) and lower flows during the warm phases (1925–1945 and 1977–2007) (Figure S2). Because we explicitly modelled the influence of the PDO, and used longer records that include at least one full PDO cycle, we could factor out the PDO's effect and conclude that the detected declining trends in surface water supplies are due to hydroclimatic changes (probably from global warming) and/or severe human impacts, and are not merely PDO phase artifacts.

[14] The effect of human impacts was strong. More actual flow records showed declines than did their corresponding naturalized records; and declines were greater in actual flows than in naturalized flows. The declines in the naturalized and unregulated gauge records reflect only hydroclimatic changes, whereas fluctuations in the actual regulated gauge records reflect both global warming effects and direct human impacts. Hence, human impact could be estimated by the difference in annualized decline rates between the actual and naturalized flows. The human impacts were typically of the same order of magnitude as the hydroclimate changes, if not greater (Table 1), confirming concerns raised by *Schindler and Donahue* [2006]. The plots of the actual and naturalized flows of the Oldman River near Lethbridge, together with their fitted multiple linear regressions and trend lines, showed the severity of human impacts in this watershed (Figure S3).

[15] Previous seminal work, *Zhang et al.* [2001], *Rood et al.* [2005, 2008], *Schindler and Donahue* [2006] and *Chen*

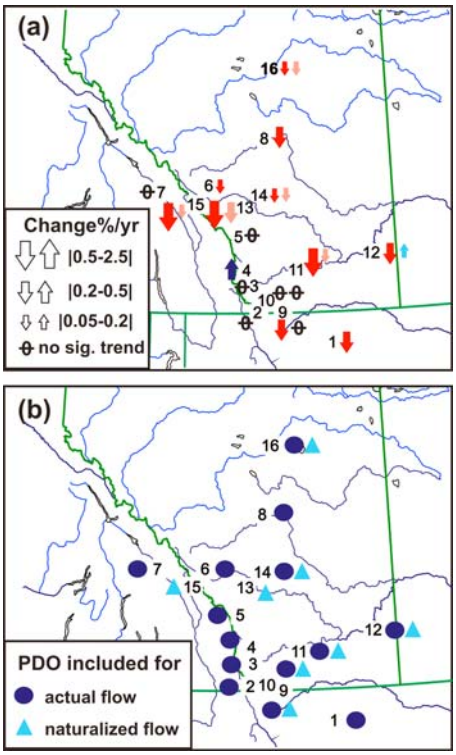

Figure 2. (a) Trends in southern Alberta mean daily streamflows. Numbers denote gauge locations named in Table 1. Red and blue arrows denote trends in actual recorded flows, pink and light blue denote trends in naturalized flows. (b) Occurrences of a PDO 0, ±1, +2 lag in the optimum subset of predictor variables. Dark blue circle (light blue triangle) denotes that the PDO was used in predicting actual (naturalized) streamflow.

and Grasby [2009], showed declining trends in southern Alberta streamflows, but did not fully address important statistical issues. *Rood et al.* [2005] noted the strong relationship between the PDO and regional streamflow, but provided no numerical method of factoring out its effect and determining if a trend remained. *Zhang et al.* [2001] and *Schindler and Donahue* [2006] did not address the issue of trend detection in the presence of the confounding effects of the PDO. Only *Zhang et al.* [2001] addressed the issue of serially correlated residuals. If the residuals are serially correlated, which is typical of streamflow data (see our observations, *Zhang et al*. [2001], and *Yue et al*. [2002]), the effective sample size of the residuals can be overestimated, causing disproportionate rejection of a no trend null hypothesis. Some climate studies [e.g., *Zheng et al.*, 1997] have used regression models with stationary and serially correlated residuals to correct this. Much current research has linked declining flow in Rocky Mountain rivers to reduced snowpack accumulation and the associated wastage of glaciers, although the latter may account for declining or augmented summer flow depending on the recent rate of glacier runoff relative to the historical contribution. Data on glacier mass balance and runoff are insufficient to determine whether the streamflow trends examined here are influenced by recent rates of glacier wastage [*Comeau et al*., 2009].

[16] The low-pass filtered streamflow data comprised a large percentage (a mean of 46.8%) of the total variability in annual flows, confirming that low-frequency variance is an important component of the hydroclimatic variability (see Table S1 for modelling details). There was no particularly favoured ARMA(p,q) model fit to the residuals, with 17 (out of 24) having relatively low complexity with $p + q \leq 5$. More complex residuals are needed to model hydrological data with its long persistence, than for regional and global temperature data which can be typically well-modeled using low-order autoregressive AR(1) residuals [*Zheng et al*., 1997; *Zheng and Basher*, 1999]. The Red Deer record was not well modeled, and should be interpreted cautiously. Although there is measurement error in these southern Alberta river discharges, ice conditions of only three to four months, HYDAT's use of ice correction coefficients and frequent peak discharge measurements in this accessible region, and our time-aggregation over the year combine to keep errors relatively low [*Shiklomanov et al.*, 2006].

[17] According to this analysis of instrumental streamflow records, future water availability in southern Alberta does not look encouraging, even without considering the expected increasing water demands of a growing economy and population. The PDO is shown to have a major impact on present-day surface water supplies. The PDO's regional importance is further underlined by tree-ring inferred streamflow reconstructions for the South Saskatchewan River Basin which show a PDO-like signal for the past six centuries, including prolonged 20–35 year low-flow regimes [*Axelson et al.*, 2009]. Because of its influence on Alberta streamflow, the status of the PDO in a warmer world under anthropogenic climate change is of serious interest. The majority of the most recent GCMs show that a warmer world will have relatively more El Niños [*IPCC*, 2007, Figure 10.16]. For instance, *Newman et al.* [2003] argued that the PDO is a reddened response to ENSO (i.e., shifted to lower frequencies), or that ENSO drives the PDO. In particular, they considered that El Niño (La Niña) drives the positive (negative) phase of the PDO. If their posited relationship holds under global warming conditions, the PDO will be in its positive phase more often and southern Alberta will see more frequent drier conditions. However, other researchers [e.g., *Zhang et al*., 1996, *Yu et al*., 2007] considered the PDO to be independent of ENSO, but that re-enforcing interactions could occur between the two oscillations. *Yu et al*. [2007] found that there occurred an enhanced response of the Pacific-North American mode when the PDO and ENSO were in the same phase; that is, when the PDO was in a positive phase and an El Niño occurred, southern Alberta experienced even warmer conditions, and presumably more evapotranspiration, than normal in a positive PDO. Hence, in this case, under global warming conditions, southern Alberta will see more severe drier conditions. Thus, regardless of the exact relationship between the PDO and ENSO, the change to a more El Niño-dominated world is expected to have major impacts (probably decreases) on southern Alberta river flow, given its strong connection to the PDO.

[18] **Acknowledgments.** This research was funded by the Natural Sciences and Engineering Research Council, EPCOR Water Services Inc. and Alberta Environment. Naturalized and void-filled stream flow data were provided by Alberta Environment, with the assistance of Michael

Seneka. We thank Xiaogu Zheng, Greg MacCulloch (WSC) and Chris Ray, and three anonymous reviewers for helpful comments which made this a better manuscript.

References

Alberta Environmental Protection (1998), South Saskatchewan River basin historical weekly natural flows 1912 to 1995, technical report, Alberta Environment, Edmonton, Canada.

Axelson, J., D. J. Sauchyn, and J. Barichivich (2009), New reconstructions of streamflow variability in the South Saskatchewan River basin from a network of tree-ring chronologies, Alberta, Canada, *Water Resour. Res.*, *45*, W09422, doi:10.1029/2008WR007639.

Brockwell, P. J., and R. A. Davis (2002), *Introduction to Time Series and Forecasting*, 2nd ed., Springer, New York.

Burn, D. H., and M. A. Hag Elnur (2002), Detection of hydrologic trends and variability, *J. Hydrol.*, *255*, 107–122, doi:10.1016/S0022-1694(01)00514-5.

Chen, Z., and S. E. Grasby (2009), Impact of decadal and century-scale oscillations on hydroclimate trend analyses, *J. Hydrol.*, *365*, 122–133, doi:10.1016/j.jhydrol.2008.11.031.

Comeau, L. E. L., A. Pietroniro, and M. N. Demuth (2009), Glacier contribution to the North and South Saskatchewan Rivers, *Hydrol. Processes*, *23*, 2640–2653, doi:10.1002/hyp.7409.

Hurvich, C. M., and C. L. Tsai (1989), Regression and time series model selection in small samples, *Biometrika*, *76*, 297–307, doi:10.1093/biomet/76.2.297.

Intergovernmental Panel on Climate Change (IPCC) (2007), *Climate Change 2007: The Physical Science Basis. Contribution of Working Group I to the Fourth Assessment Report of the Intergovernmental Panel on Climate Change*, edited by S. Solomon et al., Cambridge Univ. Press, New York.

Mantua, N. J., and S. R. Hare (2002), The Pacific Decadal Oscillation, *J. Oceanogr.*, *58*, 35–44, doi:10.1023/A:1015820616384.

Mantua, N. J., S. R. Hare, Y. Zhang, J. M. Wallace, and R. C. Francis (1997), A Pacific interdecadal climate oscillation with impacts on salmon production, *Bull. Am. Meteorol. Soc.*, *78*, 1069–1079, doi:10.1175/1520-0477(1997)078<1069:APICOW>2.0.CO;2.

Minobe, S. (1997), A 50–70 year climatic oscillation over the North Pacific and North America, *Geophys. Res. Lett.*, *24*, 683–686, doi:10.1029/97GL00504.

Newman, M., G. P. Compo, and M. A. Alexander (2003), ENSO-forced variability of the Pacific Decadal Oscillation, *J. Clim.*, *16*, 3853–3857, doi:10.1175/1520-0442(2003)016<3853:EVOTPD>2.0.CO;2.

Rood, S. B., G. M. Samuelson, J. K. Weber, and K. A. Wywrot (2005), Twentieth-century decline in streamflows from the hydrographic apex of North America, *J. Hydrol.*, *306*, 215–233, doi:10.1016/j.jhydrol.2004.09.010.

Rood, S. B., J. Pan, K. M. Gill, C. G. Franks, G. M. Samuelson, and A. Shepherd (2008), Declining summer flows of Rocky Mountain rivers: changing seasonal hydrology and probable impacts on floodplain forests, *J. Hydrol.*, *349*, 397–410, doi:10.1016/j.jhydrol.2007.11.012.

Schindler, D. W., and W. F. Donahue (2006), An impending water crisis in Canada's western prairie provinces, *Proc. Natl. Acad. Sci. U. S. A.*, *103*, 7210–7216, doi:10.1073/pnas.0601568103.

Seneka, M. (2004), Trends in historical annual flows for major rivers in Alberta, technical report, Alberta Environment, Edmonton, Canada. (Available at http://environment.gov.ab.ca/info/library/6792.pdf)

Shiklomanov, A., T. Yakovleva, R. Lammers, I. Karasev, C. Vorosmarty, and E. Linder (2006), Cold region river discharge uncertainty-estimates from large Russian rivers, *J. Hydrol.*, *326*, 231–256, doi:10.1016/j.jhydrol.2005.10.037.

Stewart, I., D. R. Cayan, and M. D. Dettinger (2005), Changes toward earlier streamflow timing across western North America, *J. Clim.*, *18*, 1136–1155, doi:10.1175/JCLI3321.1.

Wilks, D. S. (2006), *Statistical Methods in the Atmospheric Sciences*, 2nd ed., Academic, New York.

Yu, B., A. Shabbar, and F. W. Zwiers (2007), The enhanced PNA-like climate response to Pacific interannual and decadal variability, *J. Clim.*, *20*, 5285–5300, doi:10.1175/2007JCLI1480.1.

Yue, S., P. Pilon, B. Phinney, and G. Cavadias (2002), The influence of autocorrelation on the ability to detect trend in hydrological series, *Hydrol. Processes*, *16*, 1807–1829, doi:10.1002/hyp.1095.

Zhang, Y., J. M. Wallace, and N. Iwasaka (1996), Is climate variability over the North Pacific a linear response to ENSO?, *J. Clim.*, *9*, 1468–1478, doi:10.1175/1520-0442(1996)009<1468:ICVOTN>2.0.CO;2.

Zhang, X., K. D. Harvey, W. D. Hogg, and T. R. Yuzyk (2001), Trends in Canadian streamflow, *Water Resour. Res.*, *37*, 987–998, doi:10.1029/2000WR900357.

Zheng, X., and R. E. Basher (1999), Structural time series models and trend detection in global and regional temperature series, *J. Clim.*, *12*, 2347–2358, doi:10.1175/1520-0442(1999)012<2347:STSMAT>2.0.CO;2.

Zheng, X., R. E. Basher, and C. S. Thompson (1997), Trend detection in regional-mean temperature series: Maximum, minimum, mean, diurnal range, and SST, *J. Clim.*, *10*, 317–326, doi:10.1175/1520-0442(1997)010<0317:TDIRMT>2.0.CO;2.

D. J. Sauchyn and J.-M. St. Jacques, Prairie Adaptation Research Collaborative, Room 120, 2 Research Drive, University of Regina, Regina, SK, S4S 7H9 Canada. (stjacqje@uregina.ca)

Y. Zhao, Department of Mathematics and Statistics, University of Regina, Regina, SK, S4S 0A2 Canada.

Early 21st Century Projected Southern Alberta River Discharges

Suzan Lapp[1]*, Jeannine-Marie St. Jacques[1*], Yang Zhao[2] and David J. Sauchyn[1]

[1] Prairie Adaptation Research Collaborative (P.A.R.C.), Room 120, 2 Research Drive, University of Regina, Regina, Saskatchewan, Canada, S4S 7H9

[2] Department of Mathematics and Statistics, University of Regina, Regina, Saskatchewan, Canada, S4S 0A2

*Corresponding authors: lapp200s@uregina.ca, stjacqje@uregina.ca

Abstract

The 20th century hydroclimatology of southern Alberta is heavily influenced by recurring large-scale climate patterns: the Pacific Decadal Oscillation (PDO), the El Nino-Southern Oscillation (ENSO), and the Arctic Oscillation/North Atlantic Oscillation (AO/NAO). Hence, southern Alberta river discharge variability can be successfully modeled by regression techniques using these climate indices as predictors. We developed generalized-least-squares (GLS) regression equations which captured a large portion of streamflow variability. Using archived runs from global climate models, we projected the PDO, ENSO and the NAO for the first half of the 21st century. These projected climate indices were used as inputs into the GLS regression equations, giving projected southern Alberta river discharge for the early 21st century. These projections showed declining trends in southern Alberta surface water availability for 2009-2050 and increased inter-annual variability relative to the latter half of the 20th century.

Introduction

Southern Alberta hydroclimatology is heavily influenced by recurring large-scale climate patterns: the Pacific Decadal Oscillation (PDO), the El Nino-Southern Oscillation (ENSO), and the Arctic Oscillation (AO). The southern Alberta hydroclimate, like that of much of northwestern North America, displays strong periodic cycles linked to the low-frequency Pacific Decadal Oscillation (PDO) [*Mantua et al.,* 1997; *Stewart et al*., 2005; *St. Jacques et al., in press*]. The PDO is a pattern of climate variability that shifts phases on an inter-decadal time scale, usually about 20 to 35 years [*Minobe* 1997; *Mantua and Hare*, 2002]. In 1890, the PDO entered into a predominately cool (negative) phase, which continued until 1925 when a warm (positive) phase began. In 1947, the PDO shifted back into a cool phase, which lasted until 1977, whereupon a warm phase began. Winter precipitation in Alberta is higher when the PDO is in a negative phase [*Mantua et al.*, 1997; *Comeau et al*., 2009]. A strong negative relationship exists between the PDO and streamflow in south and central Alberta; therefore, these regions are wetter when the PDO is in its negative phase and drier when the PDO is positive. The higher frequency ENSO also affects the hydroclimatology of southern Alberta as precipitation and streamflow are decreased during El Niño events and increased during La Niña events [*Shabbar and Khandekar*, 1996; *Shabbar et al*., 1997; *Bonsal and Lawford*, 1999; *Bonsal et al*., 2001; *Shabbar and Skinner*, 2004; *Bonsal and Shabbar*, 2008]. The AO is a measure of the intensity of the polar vortex and is closely related to (if not the same as) the North Atlantic Oscillation (NAO) [*Wallace and Gutzler*, 1981]. A negative relationship exists between southern Prairie winter precipitation and the NAO, as the positive NAO (and AO) allows more frequent outbreaks of cold, dry Arctic air to the southern Canadian prairies [*Bonsal and Shabbar*, 2008].

Under anthropogenic global warming scenarios, southern Alberta, Canada, is projected to see decreased streamflow in this century [see Fig. 10.12, *IPCC4*, 2007, for multi-model mean run-off changes]. *St. Jacques et al*. [*in press*] analyzed southern Alberta streamflow records in order to determine if significant trends existed which could be attributable to global warming, while explicitly including the possible effects of the PDO and other interannual regional circulation anomalies to account for naturally-occurring hydroclimatic variability. They concluded that streamflows are declining at most gauges due to hydroclimatic changes (probably from global warming) and severe human impacts, which were of the same order of magnitude as the hydroclimate changes, if not greater. In the process, they developed Generalized Least Squares (GLS) regression equations which explained a large amount of the variance in southern Alberta river discharge as a function of the PDO, ENSO and the NAO. In this report, we take their best-fitting river discharge models and use them to project southern Alberta river discharge into the future. We do this by developing 21st century projections of the PDO, ENSO and NAO from archived runs of global climate models (GCMs). We then use these climate oscillation projections as inputs into the GLS regression equations to produce projected southern Alberta river discharges for 2009-2050.

Methods

River discharge modeling and projection

Five actual stream discharge records and three naturalized discharge records in southern Alberta and its environs analyzed by *St. Jacques et al*. [*in press*] were chosen for projection based on the large amount of variance explained by the GLS models built upon observed 20th century discharge data, *i.e*. high R^2 (Fig. 1, Tables 1 and 3). Two of the gauges, on the Waterton and the Marias Rivers, are on unregulated or slightly regulated river runs. Three of the gauges measure regulated flows, on the Oldman, St. Mary and Belly Rivers, and in these cases, both the observed actual flows and the reconstructed naturalized flows compiled by Alberta Environment were separately analyzed, providing an additional 6 records [*Alberta Environmental Protection,* 1998]. Four of the gauges are located in southern Alberta, with one, on the Marias River, in adjacent Montana. All records span at least 90 years.

Table 1. Details of the eight southern Alberta discharge records. Significant linear trend as assessed by *St. Jacques et al*. [*in press*]. Low-pass variance is the variance in low-frequency filtered streamflow data as a percentage of the total variability. Mean Q_t is mean daily discharge averaged over the year. The naturalized records are from the same location as the corresponding actual flow gauge.

Flow record [HYDAT or USGS code]	**Record period**	**Flow regime**	**Significant linear trend?**	**Low-pass variance**	**Gross drainage (km^2)**	**Mean Q_t (m^3/s)**
***1. Marias R. near Shelby, MT* [06099500]**	1912-2007	natural	**decreasing**	45.3%	3242	25.0
***2. Waterton R. near Waterton Park* [05AD003]**	1912-2007	natural	none	40.6%	612.7	17.6
***3. St. Mary R. at International Boundary* [05AE027]**	1903-2007	regulated	**decreasing**	51.6%	1206.4	20.2
4. St. Mary R. at International Boundary	1912-2001	naturalized	none	38.9%	1206.4	25.1
***5. Belly R. near Mountain View* [05AD005]**	1912-2007	regulated	none	38.5%	319.2	8.6
6. Belly R. near Mountain View	1912-2001	naturalized	none	38.6%	319.2	9.1
***7. Oldman R. near Lethbridge* [05AD007]**	1912-2007	regulated	**decreasing**	52.2%	17,045.6	84.6
8. Oldman R. near Lethbridge	1912-2001	naturalized	**decreasing**	44.1%	17,045.6	109.6

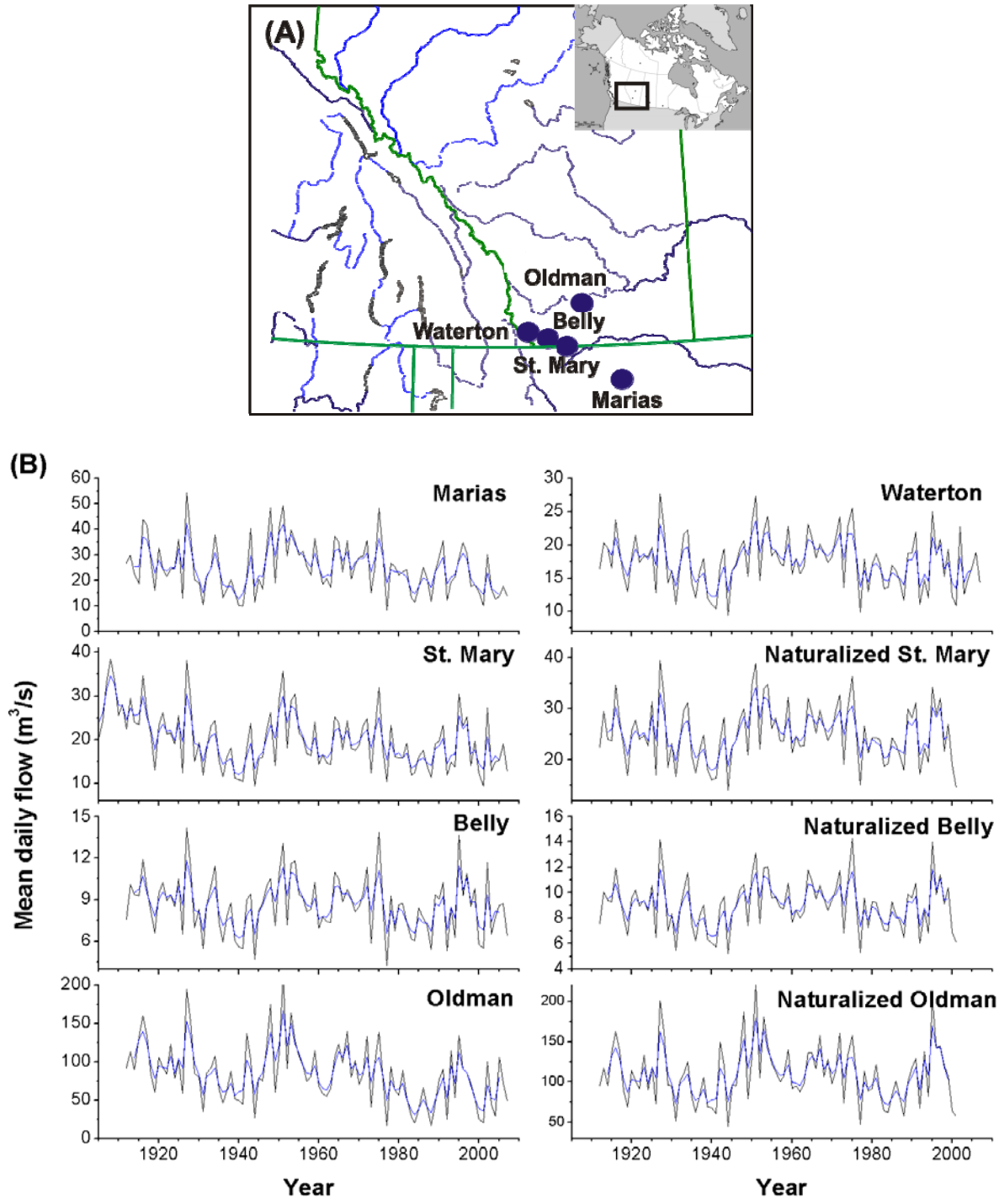

Figure 1. (A) Map of southern Alberta showing the five gauge locations. **(B)** Mean daily flows (m^3/s) (averaged over the year) of the eight discharge records at the five gauge locations for 1900-2007. Order same as that of Table 1. Black denotes mean daily flows, blue denotes the 5-year binomial smoothed flows.

We extracted the streamflow records from the Water Survey of Canada (HYDAT) (http://www.wsc.ec.gc.ca/) and the National Water Information System (http://waterdata.usgs.gov/nwis/sw) databases. In addition to gauge records from unregulated streams, a streamflow database produced by Alberta Environment provided naturalized daily flows and void-filled records to overcome the effects of human impacts and gaps in the time series [*Alberta Environmental Protection,* 1998]. Mean daily flows averaged over the year were used, because annual averaging normalizes the data by the Central Limit Theorem [*Wilks*, 2006], which allowed the use of more powerful parametric statistics. Shapiro-Wilks tests confirmed that most records were normally distributed, and that departures from normality were mild. Low-frequency variability (i.e., slightly smoothed data) was analyzed because of the associated severe socio-economic and ecological impacts of prolonged drought (Fig. 1B). High-frequency variability in precipitation and streamflow can be accommodated via conventional hazard mitigation strategies (insurance, reservoir storage, etc.), but not low frequency variability (i.e., sustained drought), which is a much more challenging climate hazard.

Following *St. Jacques et al.* [*in press*], we included as predictors in our models a linear trend and three climate indices: the Pacific Decadal Oscillation (PDO), the El Nino-Southern Oscillation, and the North Atlantic Oscillation (NAO), as a proxy for the short-duration Arctic Oscillation (AO) record. The winter averaged (Nov.-Mar.) PDO was computed from the HadSST2 dataset of sea surface temperatures (SST) following the method outlined in the appendix which closely followed the methodology of *Mantua et al*. [1997], *Zhang et al*. [1997] and *Mantua and Hare* [2002]. The annually averaged Southern Oscillation Index (SOI) and the winter averaged (Dec.-Mar.) NAO were obtained from Earth Systems Research Laboratory (National Oceanic and Atmospheric Administration, 2009, http://www.cdc.noaa.gov/ClimateIndices/). Since streamflow is naturally lagged and smoothed from precipitation by surface and subsurface hydrology, and large-scale climatic phenomena act most prominently at inter-annual time scales, the stream observations were lagged relative to the climate indices by 0, ±1, and +2 years, and a binomial smoother of five years was applied to both the stream and climate data. The climate indices and their lags showed only minor collinearity.

Generalized Least Squares (GLS) computes time series regression with serially correlated residuals and is therefore suitable for hydrological data [*Brockwell and Davis*, 2002]. Autoregressive-moving-average (ARMA(p,q)) models were fit to the residuals using a Maximum Likelihood Estimator. Open-source software from the R statistical programming language was used (http://www.r-project.org/). The statistical model used in this study is

$$Q_t = \mu + \lambda T_t + \beta_1 x_{1,t} + \ldots + \beta_k x_{k,t} + \varepsilon_t, \qquad t = 1, \ldots, L,$$

where $\{Q_t\}$ is mean daily streamflow for year t, index t runs over L years; μ is the mean streamflow over all L of these years; T_t is a linear trend with coefficient λ representing the trend to be detected; $\{x_{i,t},\ t = 1,\ldots,L\}$ is the i^{th} explanatory variable; k is the number of explanatory variables; β_i is the coefficient for the i^{th} explanatory variable; and $\{\varepsilon_t\}$ is the residual time series, which is an autoregressive-moving average process of order (p,q) (ARMA(p,q)). An optimum minimal subset of significant predictors and an optimum minimal ARMA(p,q) residual model was chosen using the corrected Akaike Information Criterion (AIC_c) goodness-of-fit statistic [*Brockwell and Davis*, 2002] applied to all predictor subsets of size ≤ 6, and for all $p \leq 8$ and $q \leq 5$. Simulation results by *Hurvich and Tsai* [1989] suggested that the AIC_c outperforms many

other model selection criteria, including the AIC and the BIC, when the number of total estimated parameters is more than 10% of the sample size. When the optimum minimal ARMA(p,q) residual model had $p + q > 5$, the model was examined for overfitting using the methods described in *sec. 8.2, Cryer and Chan* [2008] and adjusted accordingly to the ARMA(p,q) residual model with the next smallest AIC_c, if appropriate. Because in GLS regression an ARMA(p,q) model is fit to the residual error, an estimate of the error can be projected into the future and added to the extrapolated future value derived from the regression equation alone, improving the projection [*Cryer and Chan*, 2008]. Shown in Table 3 are the large improvements in the coefficient of determination, $R^{\wedge 2}$, that result in modeling the error during the period of record. We projected the residual errors for all regression models, until the projected errors' absolute value were less than 0.05.

We used ARMA processes, rather than the more general ARIMA processes [*Brockwell and Davis*, 2002]. If $\{Q_t\}$ is modelled with ARMA residuals, but really has ARIMA residuals, then erroneous trends may be found [*Woodward and Grey*, 1993]. If a process actually is ARIMA($p,1,q$) and an ARMA($p+1, q$) model is fitted to the series, its characteristic autoregressive equation is likely to have a near-unit root x (i.e., $| x - 1 | < 0.2$) [*Zheng et al*., 1997; *Zheng and Basher*, 1999; *Brockwell and Davis*, 2002]. We therefore examined the characteristic autoregressive roots of our fitted models to verify that our ARMA modeling was appropriate.

The non-zero significance of the trend coefficient λ was tested by the Neyman-Pearson statistic (RP) [*Zheng et al*., 1997] using the null model of the optimum set of explanatory variables (minus the trend variable if included in the optimum set; Table 3) versus the alternative model of the optimum set of explanatory variables together with the linear trend (if not already added). The RP is asymptotically distributed as a chi-square distribution with one degree of freedom. If the estimated RP is greater than the 0.10 percentile of $\chi^2_{(1)}$, the trend is significant at the 90% level.

How the climate indices were calculated and projected

Choice of GCMs

International modeling centers submitted to scrutiny by the wider scientific community their projections for the 21st century under different emissions scenarios together with their hindcasts of 20th century climate from 23 GCMs as part of IPCC 4 Phase 3 of the Coupled Model Intercomparison Project (CMIP3). These data are archived by the Program for Climate Model Diagnosis and Intercomparison (PCMDI) of Lawrence Livermore National Laboratory (http://www-pcmdi.llnl.gov/ipcc/about_ipcc.php). Because of the importance of recurring large-scale climate patterns (i.e., the PDO, ENSO, NAO) on surface climate, these CMIP3 runs have been critically examined for their ability to model these atmosphere-ocean climate oscillations [*Muller and Roeckner,* 2006; *Overland and Wang*, 2007; *Yu and Zwiers*, 2007; *Stoner et al*., 2009; *Wang et al*., 2010, *IPCC4*, Fig. 10.16]. *Overland and Wang* [2007], *Stoner et al*. [2009], and *Wang et al*. [2010] computed Pacific and Atlantic atmosphere-ocean climate indices from 20th century hindcast GCM SST and surface level pressure (SLP) data and compared their spatial and temporal patterns of variability to those derived from the observed 20th century climate indices. From the 23 GCMs with archived data, we chose the ones best able to simulate the PDO,

ENSO, and NAO, using similar comparisons among the 20th century observed records and the 20th century hindcasts. For the GCMs best able to simulate the PDO, we largely followed *Overland and Wang* [2007] and *Wang et al*. [2010], because they specifically examined low-frequency variability on the order of 60 years. For the GCMs best able to simulate the ENSO and NAO, we largely followed the assessment of *Stoner et al.* [2009]. We then used the intersection of the above two sets for the final set of GCMs whose runs we used for our projections of the PDO, ENSO and NAO. Our final set was CGCM3.1 (T63) [*Flato*, 2005], GDFL-CM2.1 [*Delworth et al*., 2006], UKMO-HadCM3 [*Gordon et al*., 2000; *Pope et al*., 2000], UKMO-HadGem1 [*Johns et al*., 2006; *Martin et al*., 2006], MRI-CGCM2.3.2 [*Yukimoto et al*., 2001; *Yukimoto and Noda*, 2003], and NCAR-PCM [*Washington et al*., 2000] (Table 2).

For the projections, we chose model runs under the A1B and A2 emissions scenarios. The A1B emission scenario is in the middle range of scenarios and the A2 scenario is in the high end of scenarios [*Nakicenovic et al*., 2000].

Table 2. List of chosen coupled atmosphere-ocean models, their details and number of available 21st century runs per scenario which archived the required sea surface temperature (SST) and surface level pressure (SLP) fields.

	IPCC4 Model ID	**Country**	**Atmosphere resolution**	**Ocean resolution**	**Number 21st century runs**	
					A1B	**A2**
1	**CGCM3.1(T63)**	Canada	2.8°x2.8° L31	1.4°x0.9° L29	1	0
2	**GDFL-CM2.1**	USA	2.5°x2.0° L24	1.0°x1.0° L50	1	1
3	**UKMO-HadCM3**	UK	3.75°x2.5° L15	1.25°x1.25° L20	1	1
4	**UKMO-HadGem1**	UK	1.875°x1.25° L38	(0.33-1.0°) x1.0° L40	1	1
5	**MRI-CGCM2.3.2**	Japan	2.8°x2.8° L31	(0.5-2.5°) x2.0° L23	5	5
6	**NCAR-PCM**	USA	2.8°x2.8° L18	(0.5-0.7°) x0.7° L32	2	2

Calculation of the PDO 1900-2008 and projection of the PDO post-2008

For the calculation of the PDO from the observed instrumental data, we followed the method described in *Mantua et al*. [1997], *Zhang et al*. [1997], *Mantua and Hare* [2002], and *Mantua* [*personal communication*]. Our PDO index is the leading Principal Component (PC) time series from an un-rotated EOF analysis of monthly, "residual" North Pacific SST anomalies, poleward of 20° N for the 1900-1993 time period. "Residuals" are the difference between the observed SST anomalies and the monthly mean global average SST anomaly [*Zhang et al*., 1997]. The PDO index for 1994-2008 was calculated by projecting the 1994-2008 residual SST anomalies onto the leading eigenvector or loading pattern (EOF 1) from the 1900-1993 SST data. Our main methodological divergence from *Mantua et al*. [1997] lies in our using the later and more complete sea surface temperature HadSST2 dataset [*Rayner et al.,* 2003]

(http://www.cru.uea.ac.uk/cru/data/temperature/), rather than the earlier HadSST1 [*Folland and Parker*, 1990, 1995] and the Optimally Interpolated SST data [*Reynolds and Smith*, 1995].

Following the approach of *Mantua et al*. [1997] and *Mantua* [*personal communication*] for calculating the PDO during 1994-2008, the projected PDO indices for 2009-2050 were similarly calculated by projecting the 2009-2050 residual SST anomalies from each of the GCMs onto the leading eigenvector (EOF 1) from the 1900-1993 observed SST data. Full details concerning the 20th century PDO calculation and its 21st century projection via the GCM runs are in the Appendix. All EOF analyses were performed with MATLAB©.

Model determination and validation of our PDO methodology

In order to determine the GCMs best able to simulate the PDO, we followed the approach of *Overland and Wang* [2007] and *Wang et al*. [2010]. We compared, via spatial correlation coefficients, the mapped leading eigenvector (EOF 1) from an un-rotated EOF analysis of each 20th century GCM run to the mapped EOF 1 of the observed North Pacific data ("the PDO pattern"), to determine the GCM's ability to reproduce the observed PDO spatial pattern. GCMs with correlations greater than 0.7 with the observed North Pacific EOF 1 were considered suitable for this analysis. Using Multi-taper spectral analysis (MTM), we also confirmed that the leading PC time series of each 20th century GCM run showed similar temporal variability as the observed PDO index (results not shown).

In order to validate our PDO projection method and to explore patterns of projected 21st century North Pacific ocean variability, for each chosen GCM and for each of its archived 21st century runs, we performed a similar un-rotated EOF analysis of the 2000-2050 residual projected SST anomalies. The mapped EOF 1 and EOF 2 were then compared by spatial correlation to the PDO loading pattern from the 1900-1993 observed data.

Calculation and projections of the SOI and NAO

We calculated the SOI as the difference between monthly mean SLP at Tahiti, Polynesia (17.5° S, 149.6° W), and Darwin, Australia (12.4° N, 130.9° E), with the difference normalized relative to 1951-1980 [*Ropelewski and Jones*, 1987]. The SOI was projected using the same formula with the station monthly mean SLP data replaced by SLP monthly mean data from the corresponding GCM grid cells. For validation purposes, the SOI was calculated in the same fashion using the 20th century hindcasts for each GCM. We also confirmed with MTM spectral analysis that the hindcast SOI of each 20th century GCM run showed similar temporal variability as the observed SOI (results not shown).

We calculated the NAO index as the difference between monthly mean SLP at Gibraltar, Spain (36.1° N, 5.2° W), and Reykjavik, Iceland (64.1° N, 21.6° W), each normalized relative to 1951-1980 before differencing [*Jones et al*., 1997]. The NAO was projected using the same formula with the station monthly mean SLP data replaced by SLP monthly mean data from the corresponding GCM grid cells. For validation purposes, the NAO was calculated in the same fashion using the 20th century hindcasts for each GCM. We also confirmed with MTM spectral analysis that the hindcast NAO of each 20th century GCM run showed similar temporal variability as the observed NAO index (results not shown).

Results

GLS river discharge modeling

The GLS regression analysis showed a regional pattern of declining flows in the 20th century (Table 3 and Figure 2). Six of the eight models revealed significant declining trends, with the exceptions being the naturalized St. Mary and the naturalized Belly discharge records, which showed no trends. Both of the gauge records in relatively undisturbed watersheds, the Marias and Waterton Rivers, showed significant declines, as did the naturalized Oldman River, which indicates that the declines are not purely due to direct human impact, but also to hydroclimatic causes, presumably global warming. The current year PDO or a lead or lag was the explanatory variable that always appeared in the optimum predictor set. Because the predictor variables were standardized to zero mean and unit standard deviation, the relative importance of the predictors could be assessed by comparing the regression coefficients. This showed that the declining trend and the PDO were the most influential predictors. The majority of the 20th century variance was captured by the GLS regression models. The mean R^2 was 0.56, with R^2 computed as 1 – (sum-of-squares of simple regression residuals/total-sum-of-squares), *i.e*. without modeled error adjustment (Table 3). When R^2 was computed with the modeled error adjustment, its mean was 0.69. Plots of the discharge records, together with the fitted regression models, show that the low frequency variance was captured well, with the extreme flows being captured less well (Fig. 2). ARMA(p, q) models where $p \geq 2$ most frequently fitted the error terms, showing the importance of multi-year persistence. All records had no near-unit autoregressive roots, which suggested that ARMA residuals are appropriate.

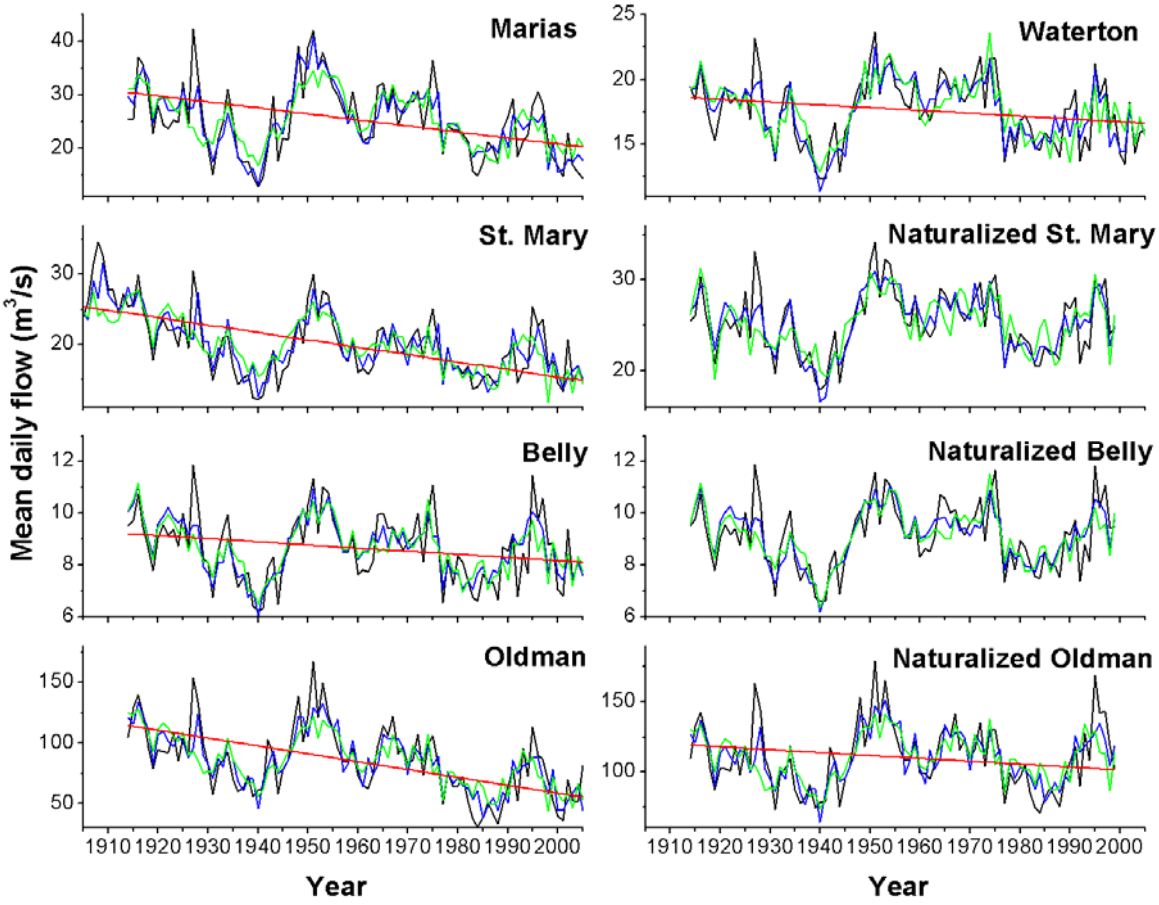

Figure 2. Plots of the eight southern Alberta flow records, smoothed by 5-point binomial filters (black lines), together with fitted multiple linear GLS regressions with ARMA modeled error terms (blue), fitted multiple linear GLS regressions without the error terms (green), and significant trend lines (red). Mean daily flows (m^3/s) averaged over the year are presented.

Table 3. Identification of the optimum generalized least squares (GLS) equations and residual models for southern Alberta streamflow. AIC_c: corrected Akaike Information Criterion. Predictor variables are standardized to zero mean and unit standard deviation; discharge Q_t is centered to zero mean. 0, ±1, +2 year lags of climate indices included in analysis. P1: climate leads streamflow 1 year. P2: climate leads streamflow 2 years. N1: climate lags streamflow 1 year. RP: Neyman-Pearson statistic (results significant at the 10% level in bold).

Flow record	R^{2*} (regular)	R^{2**} (innovations)	AIC_c	GLS equation	Residual model	RP (*p*-level)
1. Marias River	0.56	0.74	526.2	$Q_t = 0.21 - 3.0*trend - 2.07*PDO - 1.06*NAO_{P1} - 1.21*PDO_{P1} - 2.06*PDO_{P2} - 2.44*SOI_{P2}$	ARMA(2,3)	**30.0 ($4.3 \times e^{-8}$)**
2. Waterton River	0.57	0.66	359.4	$Q_t = 0.06 - 0.58*trend - 1.06*PDO + 0.57*SOI_{N1} - 1.06*PDO_{P2} - 0.69*SOI_{P2}$	ARMA(1,2)	**12.8 (0.0003)**
3. Actual St. Mary River	0.61	0.75	492.6	$Q_t = -0.03 - 3.10*trend - 1.52*PDO + 0.80*NAO_{P2} - 1.31*PDO_{P2} - 1.50*SOI_{P2}$	ARMA(0,3)	**22.6 ($2.0 \times e^{-6}$)**
4. Naturalized St. Mary River	0.51	0.71	393.5	$Q_t = -0.03 - 1.55*PDO + 0.76*SOI - 0.90*NAO_{N1} + 1.09*NAO_{P2} - 0.98*PDO_{P2} - 1.04*SOI_{P2}$	ARMA(3,2)	0.58 (0.45)
5. Actual Belly River	0.55	0.64	239.1	$Q_t = 0.01 - 0.32*trend - 0.40*PDO + 0.34*SOI_{N1} + 0.31*NAO_{P2} - 0.47*PDO_{P2} - 0.35*SOI_{P2}$	ARMA(1,2)	**15.3 ($9.0 \times e^{-5}$)**
6. Naturalized Belly River	0.57	0.67	214.0	$Q_t = 0.002 - 0.37*PDO + 0.24*SOI + 0.31*SOI_{N1} + 0.24*NAO_{P2} - 0.50*PDO_{P2} - 0.34*SOI_{P2}$	ARMA(2,1)	0.02 (0.89)
7. Actual Oldman River	0.62	0.73	787.3	$Q_t = 0.11 - 17.17*trend - 9.25*PDO - 9.52*PDO_{P2} - 9.75*SOI_{P2}$	ARMA(2,3)	**19.7 ($9.0 \times e^{-6}$)**
8. Naturalized Oldman River	0.49	0.65	729.0	$Q_t = -0.24 - 5.16*trend - 8.38*PDO - 10.02*PDO_{P2} - 10.19*SOI_{P2}$	ARMA(2,3)	**3.6 (0.06)**

* R^2 computed as 1 – (sum-of-squares of regression residuals/total-sum-of-squares), *i.e.* without modeled error adjustment.

** R^2 computed with the modeled error adjustment.

PDO projections

The six chosen models reproduce the spatial pattern of the observed 20th century PDO well (Fig. 3). However, the hindcast PDOs typically explained more North Pacific residual variance than they ought to have in comparison to actual observed variability (with the exception of the HadGEM1 model). Our model choices are validated by the EOF analyses of the projected 2000-2050 residual SSTs (Figs. 4 and 5). For the A1B emission scenario, all six of the models with one exception produced a recognizable PDO spatial pattern as their EOF 1. The single exception was GFDL 2.1 (run 1) whose EOF 1 appeared to be a polar amplification pattern and whose EOF 2 produced a recognizable PDO pattern. For the A2 emission scenario, all five of the models produced a recognizable PDO spatial pattern as their EOF 1 (CGCM3.1(T63) had no A2 runs). Similar to the hindcast PDOs, the early 21st century PDOs typically explained more North Pacific residual variance than they ought to have.

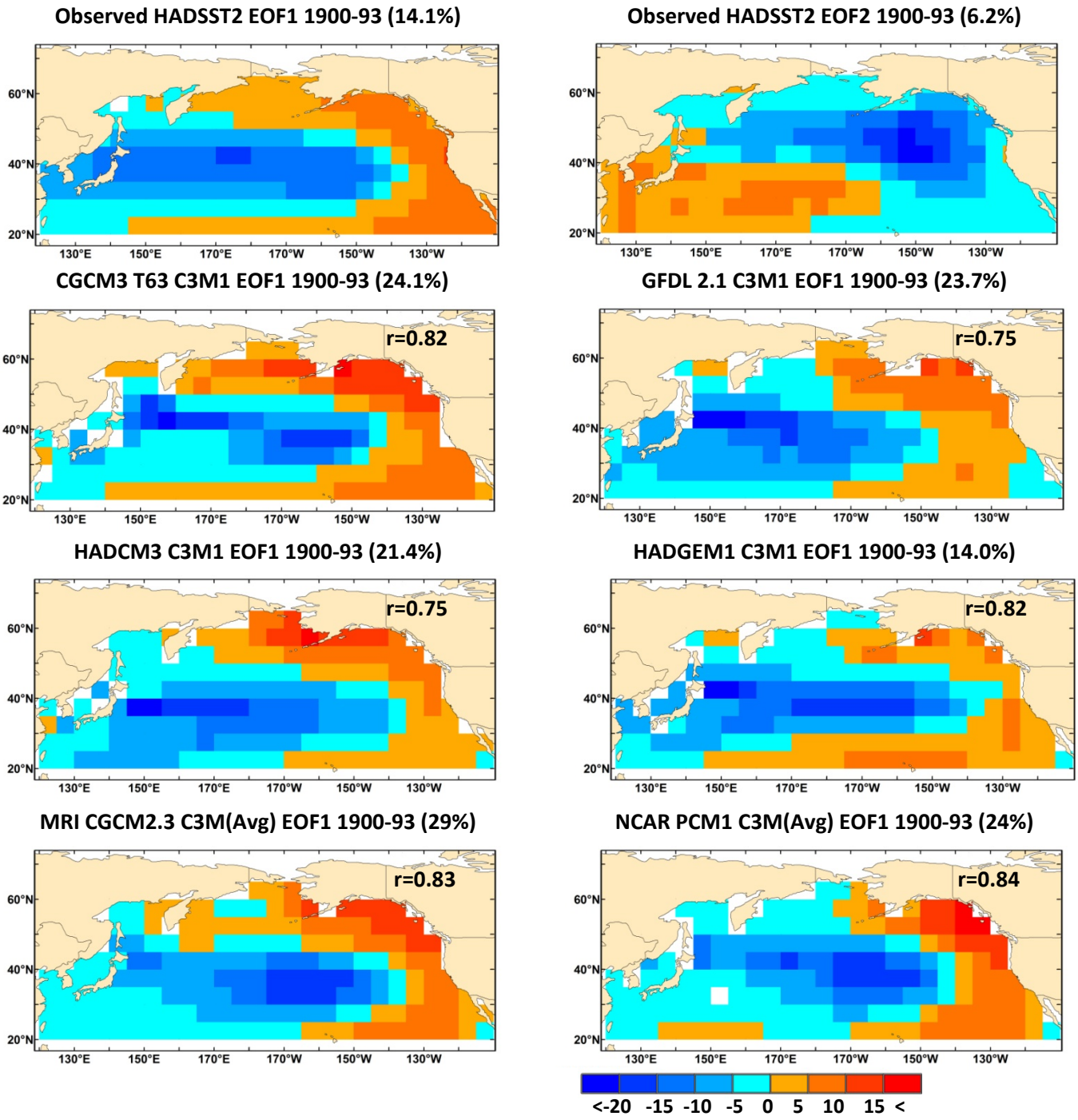

Figure 3. The spatial patterns of the leading EOFs of North Pacific SST residuals for the six chosen models, based upon the 20th century hindcasts, together with that from the PDO (i.e., EOF 1 from the observed 1900-1993 HadSST2 data). The percent variance explained is given after the model name; spatial correlation coefficients indicated in the lower right hand corner. Color scale shows PCA loadings (x 100).

Early 21st century (2000-2050) PDO projections showed a shift towards more occurrences of the positive phase PDO for both emissions scenarios (Fig. 6 and Table 4). This can be seen by comparing the all-model 1900-1999 hindcast mean to the all-model 2000-2050 mean (Table 4). Under the more severe A2 emissions scenario, the shift towards more positive phase PDO occurrences was more pronounced. Comparison of the all-model 1900-1999 hindcast means to the actual 1900-1999 observed mean PDO index showed that that the GCMs reasonably simulated mean PDO state, although the A2 emission hindcasts produced more negative phase PDO occurrences than were actually observed.

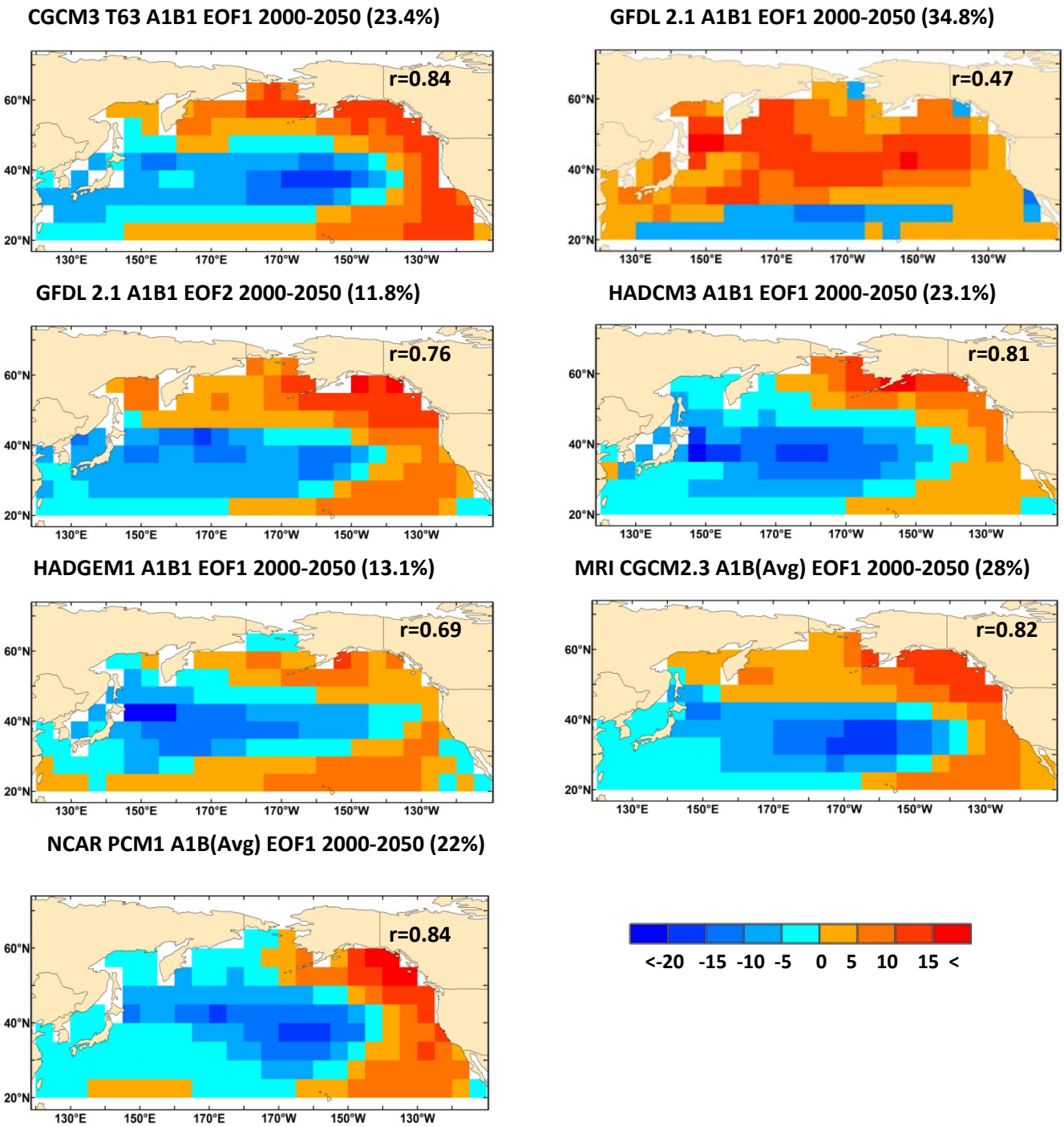

Figure 4. The spatial patterns of the first EOFs of the 2000-2050 North Pacific projected SST residuals from the six chosen models, under the 21th century A1B emissions scenario, together with EOF 2 from the GFDL 2.1 model (see text). If multiple runs were available for a model, ensemble means are presented. The percent variance explained is given after the model name; spatial correlation coefficients indicated in the upper right hand corner. Color scale shows PCA loadings (x 100).

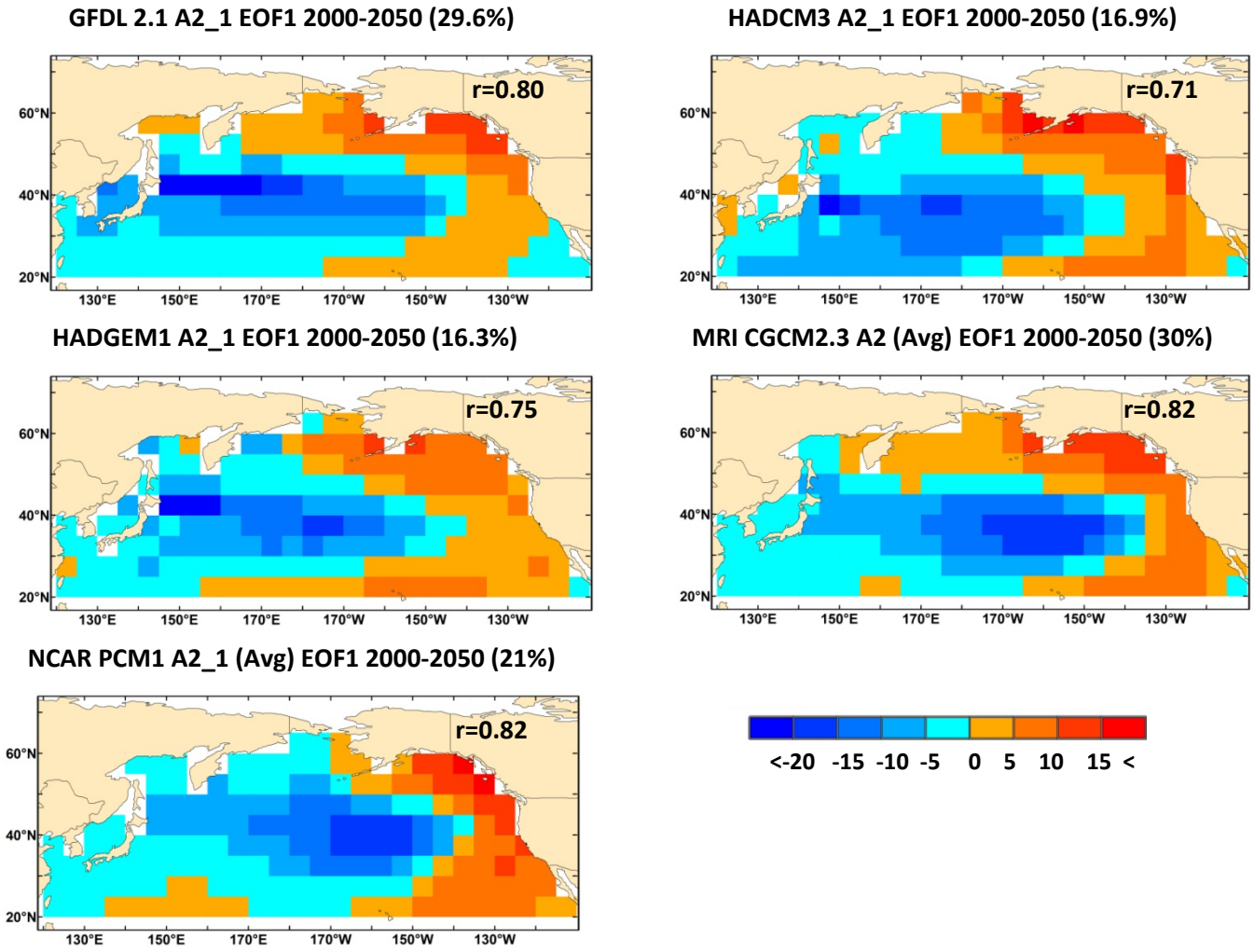

Figure 5. The spatial patterns of the first EOFs of the 2000-2050 North Pacific projected SST residuals from the five models with available runs, under the 21th century A2 emissions scenario. If multiple runs were available for a model, ensemble means are presented. The percent variance explained is given after the model name; spatial correlation coefficients indicated in the lower right hand corner. Color scale shows PCA loadings (x 100).

Table 4. 20th century observed mean climate indices and multi-model mean climate indices for the 20th century hindcasts and for the 21st century projections under the A1B and A2 emission scenarios. *CGCM3.1(T63) had no A2 run, therefore its hindcast run was dropped from the multi-model hindcast mean.

	PDO		SOI		NAO	
Emission scenario	**A1B**	**A2**	**A1B**	**A2**	**A1B**	**A2**
Observed mean 1900-1999	*0.168		-0.089		0.485	
All-model 1900-1999 hindcast mean	-0.094	-0.141	0.045	0.006	-0.049	-0.066
All-model 2000-2050 mean	0.109	0.237	0.011	-0.039	0.114	0.058

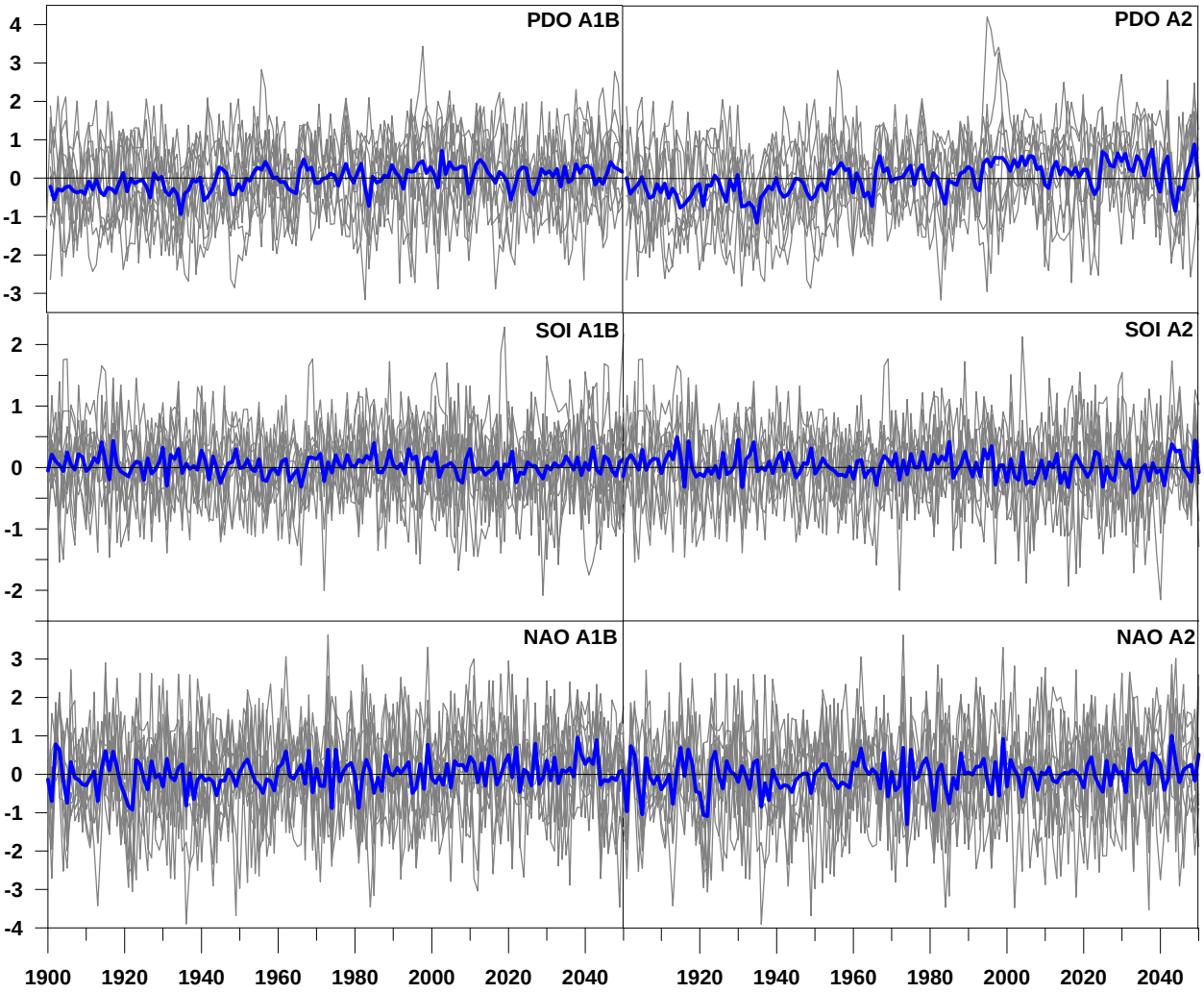

Figure 6. PDO, SOI and NAO indices 1900-1999 calculated from 20th century hindcasts, together with projections for 2000-2050 for the A1B and A2 emission scenarios. The grey lines are the individual model runs and the heavy blue lines are all-model means of the GCM runs.

SOI and NAO projections

Early 21st century (2000-2050) SOI projections showed a shift towards a climate with more occurrences of El Niño (negative SOI) and decreases in the occurrences of La Niña (positive SOI) for both emissions scenarios (Fig. 6 and Table 4). This can be seen by comparing the all-model 1900-1999 hindcast mean to the all-model 2000-2050 mean (Table 4). Under the more severe A2 emissions scenario, the shift towards more El Niño occurrences was more pronounced, than under the more moderate A1B scenario. Comparison of the all-model 1900-1999 hindcast means to the actual 1900-1999 observed mean SOI index showed that that the GCMs had a bias towards simulating more La Niña events than actually happened, with the A2 hindcasts being less biased than the A1B hindcasts.

Early 21st century (2000-2050) NAO projections showed a shift towards a climate with more occurrences of the positive phase of the NAO (positive AO) and decreases in the occurrences of the negative NAO (negative AO) for both emissions scenarios (Fig. 6 and Table 4). This can be seen by comparing the all-model 1900-1999 hindcast mean to the all-model 2000-2050 mean (Table 4). Comparison of the all-model 1900-1999 hindcast means to the actual 1900-1999 observed mean NAO index showed that that the GCMs had a problem reproducing the NAO accurately, having a marked bias towards simulating more negative NAO events than actually happened for both emissions scenarios.

Southern Alberta projected streamflows

Our GLS regression modeling approach based upon GCM projected climate indices indicates declining trends in projected southern Alberta surface water availability for the first half of the 21st century (Fig. 7). Six of the eight models showed declining trends in the all-model mean projections; the exceptions are the naturalized St. Mary and the naturalized Belly discharge records, which showed no trends. Both of the gauge records on relatively undisturbed watersheds, the Marias and Waterton Rivers, showed projected declines, as did the naturalized Oldman River, which indicates that the declines are not purely due to projected continued direct human impact, but also to global warming. As well, these three projections of records with little direct human impact showed roughly the same decline rates. At all three regulated gauges, the all-model mean projections based upon the actual flows showed much steeper declines than the all-model mean projections based upon the naturalized flows, showing that severe direct human impacts are projected to continue. The all-model mean projection based upon the actual flow record for the Oldman River at Lethbridge showed the steepest rate of decline, approaching zero flow at the mid-century. There were no apparent differences between the two emissions scenarios (Figs 7A and 7B). Visual comparison of the observed discharge variability to the variability of the individual 20th century hindcast runs showed that the GCMs are reasonably capturing the natural variability of the discharge records.

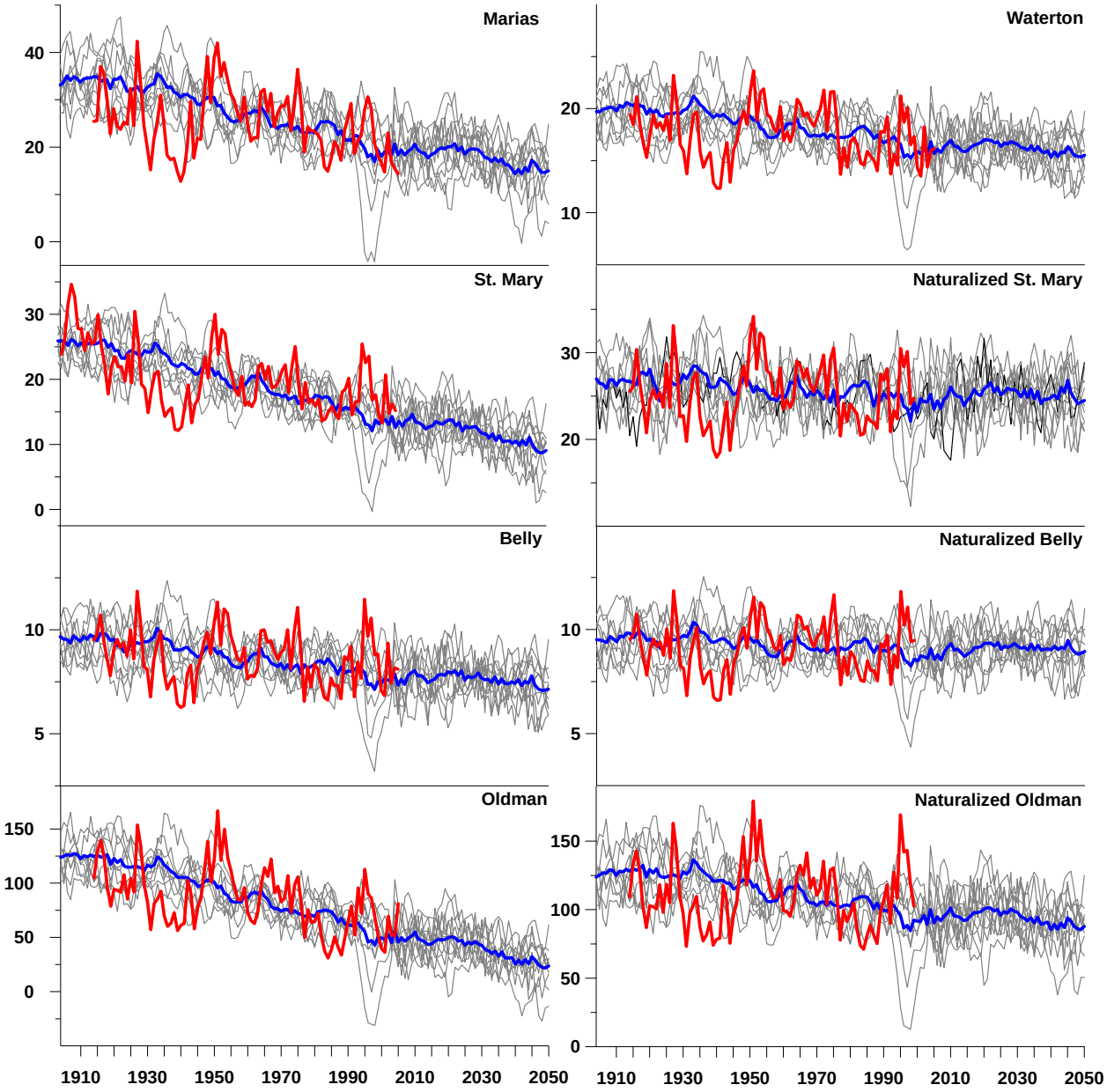

Figure 7. (A) Southern Alberta river projections 2000-2050 under the A1B emissions scenario, together with observed records (1905-2005), and 20th century river hindcasts (1900-1999) (daily mean flows (m^3/s), averaged over the year). The grey lines are the individual model runs, the heavy blue lines are all-model means of the GCM runs, and the heavy red lines are the observed river records.

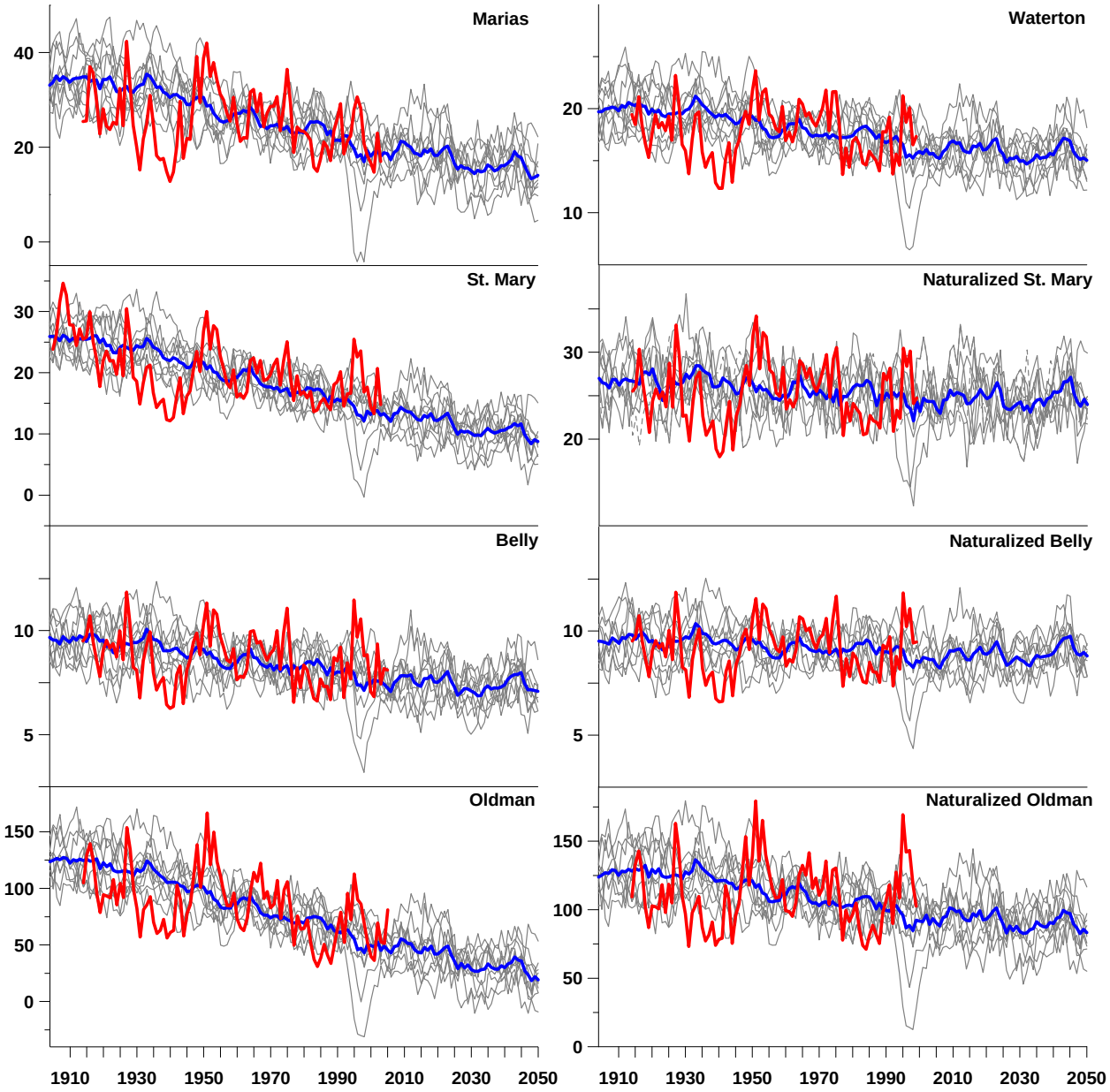

Figure 7. (B) Southern Alberta river projections 2000-2050 under the A2 emissions scenario, together with observed records (1905-2005), and 20th century river hindcasts (1900-1999) (daily mean flows (m^3/s), averaged over the year). The grey lines are the individual model runs, the heavy blue lines are all-model means of the GCM runs, and the heavy red lines are the observed river records.

Discussion

Like previous work [e.g., *Zhang et al*., 2001; *Rood et al.,* 2005; 2008; *Schindler and Donahue*, 2006; *St.Jacques et al., in press*], this study suggests a worsening availability of surface water supplies for southern Alberta for the early 21st century. Also similar to previous work, this study suggests that any deleterious effects of global warming on surface water supplies are only compounded by the drawdown effects of direct human impacts, which are of at least a similar order of magnitude. This is particularly illustrated by the projection of the all-model mean of the actual flow of the Oldman River at Lethbridge, an acknowledged over-allocated system, which is projected to reach nearly zero flows by mid-century (Fig. 7).

Unlike previous forecasts of Alberta's future surface water supplies, our work is not based simply on an extrapolation of recent streamflow trends (*Rood et al.,* 2005; 2008; *Schindler and Donahue*, 2006) or in projects shifts in mean climate conditions. The projections presented here are based on an understanding of the climate forcing of regional hydroclimatic variability and a corresponding statistical model that captures a large proportion of this variability. This approach is not without precedent as *Stewart et al.* [2004] developed a similar ordinary least squares regression based projection of changes in western North American snowmelt runoff timing. Future mean annual streamflow in the SSRB has been previously projected (Lapp et al., 2009) by applying climate change scenarios to models of watershed hydrology. Whereas this approach gives the expected shift in mean annual streamflow between 30-year periods, our method captures the important interannual to interdecadal variability related to teleconnections in hemisphere scale coupled circulation of the ocean and atmosphere. Therefore, in addition to projecting streamflow trends, we are able to present in this report future simulations of the important forcing of hydroclimatic variability and the resulting interannual to interdecadal variability in streamflow at selected gauges. Although the exact timing of departures from mean flow has no meaning, since every simulation is a unique sequence of annual flows, the frequency, magnitude and duration of extreme flows can be characterized from the multiple climate model simulations. They show some large and sustained departures from mean flows from the 1990s through to 2050. The variability exceeds that in the baseline period 1961-90, and the mid to latter 20th century in general. There is also, however, considerable flow variability in the early part of the 20th century. The large and sustained negative departures in some of the simulations are especially concerning, especially in the future, since these are departures from a declining mean flow.

The declining trends and the PDO terms were the most influential predictors among those examined (Table 3). Included in the declining trends are the direct human impacts of water withdrawals and change in regional hydroclimate arising from a warming climate. This study found a greater prevalence of declining significant trends than the earlier study of *St. Jacques et al.* [*in press*] using most of the same discharge records. We attribute this to our use of the later compiled and more complete HadSST2 dataset in our construction of the PDO index, which we think more accurately represents the historic North Pacific pattern of variability. *St. Jacques et al.* [*in press*] used Mantua's PDO index in their analysis which was based upon the earlier and less complete HadSST1 dataset.

Our analysis required that output from each GCM be available for both the 20th century and 21st century in concurrent runs; often GCMs' have several runs for the 20th century but with only one

or two of these runs continuing through the 21st century for the different emission scenarios. *Overland and Wang* [2007] and *Stoner et al.* [2009] considered the GFDL 2.0 model to produce acceptable PDO simulations both temporally and spatially, however our results differ. *Overland and Wang* [2007] compared the first EOF spatial pattern using the 20th century hindcast GCM ensemble mean to the observed North Pacific EOF 1 spatial pattern, rather than each individual run as only one run continued through the 21st century. We conducted an EOF analysis on this GFDL 2.0 run for the 20th century hindcast and found that EOF 1 correlated with HadSST2 EOF2 and EOF 2 correlated with HadSST2 EOF 1, therefore we excluded this GCM from the analysis. *Stoner et al.* [2009] also concluded that CGCM3 (T63) was incapable of producing the ENSO time series using tropical SSTs, however after comparing the CGCM3 (T63) SOI 20th century hindcast temporal variability with the observed SOI variability through MTM we ruled the model as capable (results not shown). Overall, after comparing the spatial and temporal variability of the 20th century hindcast PDO, SOI and NAO to the observed indices, we concluded the HadCM3 and CGCM3 (T63) ranked as the top two models.

How realistic are the moderate A1B and severe A2 emission scenarios used in this study? Recent research [*van Vuuren and Riahi*, 2008] compared actual measured emissions to the IPCC Special Report on Emissions Scenarios (SRES) forecast rates and showed that thus far, for 1990-2006, a high emissions scenario has been most appropriate. The growth rate of global emissions after 2000 has been about 3%, whereas the forecast growth rates under SRES had ranged from between 1.4% and 3.4%.

Because of its influence on northwestern North American river discharge, the status of the PDO in a warmer world under anthropogenic climate change is of serious interest. This study confirmed the result of the strong negative relationship between the PDO and southern Alberta precipitation and streamflow found by many researchers [*Mantua et al.,* 1997; *Stewart et al*., 2005; *St. Jacques et al., in press*]. The ability of the current highest-resolution GCMs to project the future status of the PDO is just beginning to be examined. As far as we know, our present study is the first to explicitly project the PDO. Its finding of an increase in positive phase PDO events for the early 21st century leads to concern for future regional surface water availability. *Overland and Wang* [2007] and *Wang et al.* [2010] examined the closely related question of when the anthropogenic global warming trend will surpass the natural variability of the North Pacific Region under the A1B emissions scenario. Their EOF analysis used direct North Pacific SST anomalies, rather than the residuals after the global ocean warming trend had been removed, as did our analysis and that of *Mantua et al.* [1997], and *Zhang et al.* [1997]. Importantly, *Overland and Wang* [2007] and *Wang et al.* [2010] found that the global warming trend will surpass the natural variability circa 2040-2050, leading towards a weaker meridional temperature gradient in the North Pacific Region. Because of this result, we do not project the PDO or southern Alberta streamflow past 2050.

The mechanism by which the PDO, or the zonal dipole in North Pacific SSTs, affects the hydroclimatology of the Pacific Northwest and interior is thru control of the position of the sub-polar jet, which brings winter storms and precipitation, as it crosses over the edge of the continent [*Gershunov and Barnett*, 1998]. We presume that the same mechanism will continue to operate in the early 21st century in the presence of an increased global warming trend, as it operated in the 20th century in the presence of an increasing global warming trend in surface air

temperatures and SSTs [*Kaplan et al*., 2000]. Hence, it is reasonable to forecast the PDO by projecting the 2000-2050 residual SST anomalies from each of the GCMs onto the leading eigenvector from the 1900-1993 observed HadSST2 data. However, it seems uncertain to assume that this mechanism will operate as before when the global warming trend surpasses the natural North Pacific variability circa 2040-2050 [*Overland and Wang,* 2007; and *Wang et al.,* 2010].

Like the PDO, the status of ENSO in a warmer world under anthropogenic climate change will also have negative repercussions on southern Alberta streamflow. The majority of the most recent GCMs show that a warmer world will have relatively more El Niños by the late 21st century under the A2 emission scenario [Fig. 10.16*, IPCC4*, 2007]. This accords with our multi-model mean shift towards more frequent El Niños for the early 21st century for both the A1B and A2 emissions scenarios.

It is unknown whether the PDO is independent of ENSO or not, and this is an active area of research [*IPCC4*, 2007]. Some researchers [e.g., *Newman et al.,* 2003; *Schneider and Cornuelle*, 2005; *Newman*, 2007] have argued that ENSO drives the PDO, i.e., that El Niño (La Niña) drives the positive (negative) phase of the PDO. If true, then since there will be more El Niño events under global warming, the PDO will be in its positive phase more often (which accords with this study's projections) and southern Alberta will see more frequent drier conditions. However, other researchers [e.g., *Zhang et al*., 1996, *Yu et al*., 2007] have considered the PDO to be independent of ENSO, but that re-enforcing interactions could occur between the two oscillations. *Gershunov and Barnett* [1998] and *Yu et al*. [2007] found that there occurred an enhanced response of the Pacific-North American mode when the PDO and ENSO were in the same phase; that is, when the PDO was in a positive phase and an El Niño occurred, southern Alberta experienced even warmer conditions, and presumably more evapotranspiration, than normal in a positive PDO. Hence, in this case, under global warming conditions we project the PDO to be in its positive phase more often and there to be more frequent El Niños, then southern Alberta will see more frequent and more severe drier conditions. Thus, regardless of the precise relationship between the PDO and ENSO, the change to a more El Niño-dominated and a more positive PDO-dominated world is expected to cause decreased southern Alberta river flow in the 21st century.

The NAO/AO is an important contributor to the Northern Hemisphere climate variability [*Shabbar and Bonsal*, 2003; *Min et al*., 2009]. We projected that the future climate will exhibit a more positive NAO pattern than that experienced during the observed period, which should result in drier winter conditions in southern Alberta [*Shabbar and Bonsal*, 2003; *Shabbar and Bonsal*, 2004; *Bonsal and Shabbar*, 2008]. This result is in good accord with the literature reviewed by the *IPCC4* [2007] (see Fig. 10.17). It is suggested that the projected increasing NAO index is due to polar vortex intensification caused by tropospheric warming and stratospheric cooling [*IPCC4,* 2007]. However, we found that our all-model 1900-1999 hindcast mean was quite different from the observed 1900-1999 mean NAO index, leading to concerns as to how well the GCMs are capturing the NAO's behavior. We are not alone in this concern. *Stoner et al.* [2009] found that SLP fields tended to be more influenced by local features compared to higher level data, which is possibly the source of the inconsistency between our GCM hindcast all-model NAO and the observed NAO index.

Acknowledgments

We thank N.J. Mantua for his help concerning details of the PDO computation.

Appendix

Full details of how the PDO was calculated are given below. We followed most of the details for computing the PDO index in *Zhang et al.* [1997] and at ftp://ftp.atmos.washington.edu/mantua/pdofiles/; we note any differences.

Observed PDO for 1900-2008

Data used:

Monthly SST centered anomalies from the HadSST2 dataset for 1900-2008 (http://www.cru.uea.ac.uk/cru/data/temperature/). The data are arranged as a 5^o by 5^o grid covering the global ocean, with the first grid point centered at 177.5W and 87.5N. These SSTs are standardized at each grid point by subtracting the monthly means for 1961-1990 calculated from each individual grid point. 2009 data were not yet available when this analysis was performed. We used the HadSST2 dataset rather than the HadSST1 dataset used by *Mantua et al.* [1997] because it is a later, improved version. When the HadSST2 dataset was downloaded, no 2009 data were available.

Method

(1) Let the North_Pacific_SST_grid be defined as all grid points in the North Pacific Ocean north of 20^o N and south of 65^o N in the HadSST2 dataset. 197 grid points in total for this set. Let the North_Pacific_SST be defined the field of SST anomalies (from HadSST2) from the grid points in North_Pacific_SST_grid, covering 1900-2008. So the field consists of 197 time series, each of length 1308 (12 months, 109 years).

(2) Let the Global_Ocean_SST_grid be defined as all grid points in the global ocean north of 35^o S and south of 75^o N in the HadSST2 dataset. A large portion of the Southern Ocean is deleted because there simply is not enough SST data for it spanning 1900-2008. 1177 grid points in total for this set.

(3) Using Global_Ocean_SST_grid locations, calculate a monthly mean global SST anomaly time series "Observed_global_mean" for 1900-2008, i.e., for each month in each year, compute the mean SST anomaly over the entire global ocean. Observed_global_mean has length 1308 (12 months, 109 years).

(4) Create a "Residual observed SST anomaly" field for the North Pacific by subtracting component-wise the Observed_global_ mean time series from each individual SST time series in North_Pacific_SST.

(5) Truncate the Residual observed SST anomaly field to consist of data only from 1900-1993. Call this field "1900-1993 Residual observed SST anomaly." The data from each of the 197 grid locations is now a time series of length 1128 (12 months, 94 years). Perform EOF analysis of the 1900-1993 Residual observed SST anomaly field using the

temporal covariance matrix, without any normalization or rotation [*Wilks*, 2006; *Bjornsson and Venegas*, 1997]. In performing the EOF analysis, missing data points are set to zero. Owing to the paucity of data from the North Pacific in the earlier decades of the 1900s, this is an issue that must be addressed. The PDO index for 1900-1993 is the leading PC time series or PC 1 from this analysis. The leading eigenvector or loading pattern mapped produces the 1900-1993 PDO pattern in the North Pacific (Fig. 3).

(6) PDO index values for 1994-2008 are computed differently, following the methodology of *Mantua et al.* [1998]. Truncate the Residual observed SST anomaly field to consist of data only from 1994-2008. Call this field "1994-2008 Residual observed SST anomaly." The data from each of the 197 grid locations is now a time series of length 192 (12 months, 16 years). Project the 1994-2008 Residual observed SST anomaly field onto the leading eigenvector from step (5). This gives the PDO index for 1994-2008.

(7) The monthly PC time series was normalized relative to 1961-1990 (i.e., centered by subtracting the mean, and then divided by the standard deviation) and winter (November-March) indices are extracted and averaged together.

Projected PDO for 2009-2050

This is computed analogously to step (6) above. For each chosen GCM and for each of its archived 20^{th} and 21^{st} century runs compute a "1994-2050 Residual projected SST anomaly field" for the North Pacific for 1994-2050, following the steps described above and making the appropriate changes. Interpolation of the GCM SSTs to the same 5^{o} by 5^{o} grid used by the Hadley Centre was necessary in all cases, using the spline method in MATLAB. The data from each of the 197 grid locations is now a time series of length 492 (12 months, 42 years). Project the 1994-2050 Residual projected SST anomaly field onto the leading eigenvector from step (5) from the EOF analysis of the 1900-1993 observed HadSST2 data. This gives the PDO index for 1994-2050.

References

Alberta Environmental Protection (1998), South Saskatchewan River basin historical weekly natural flows 1912 to 1995. Technical Report Alberta Environment.

Bjornsson, H., and S.A. Venegas (1997). *A manual for EOF and SVD analyses of climatic data.* Technical Report No. 97-1 Department of Atmospheric and Oceanic Sciences and Centre for Climate and Global Change Research, McGill University, Montreal, Quebec.

Bonsal, B., and R.G. Lawford (1999), Teleconnections between El Niño and La Niña events and summer extended dry spells on the Canadian prairies, *Int. J. Climatol.,* 19, 1445-1458.

Bonsal, B., A. Shabbar, and K. Higuchi (2001), Impacts of low frequency variability modes on Canadian winter temperature, *Int. J. Climatol.,* 21, 95-108.

Bonsal, B., and A. Shabbar (2008), Impacts of large-scale circulation variability on low streamflows over Canada: a review, *Can. Water. Res. J.,* 33, 137-154.

Brockwell, P.J., and R.A. Davis (2002), *Introduction to time series and forcasting*, 2nd *ed*., Springer-Verlag, New York.

Comeau, L.E.L., A. Pietroniro and M.N. Demuth (2009), Glacier contribution to the North and South Saskatchewan Rivers, *Hydro. Proc.,* 23, 2640-2653.

Cryer, J.D. and K.-S. Chan (2008), *Time series analysis with applications in R,* 2nd *ed.,* Springer-Verlag, New York.

Delworth, T.L., A. Rosati, R.J. Stouffer, K.W. Dixon, J. Dunne, K. Findell, P. Ginoux, A. Gnanadesikan, C.T. Gordon, S.M. Griffies, R. Gudgel, M.J. Harrison, I.M. Held, R.S. Hemler, L.W. Horowitz, S.A. Klein, T.R. Knutson, S.-J. Lin, P.C.D. Milly, V. Ramaswamy, M.D. Schwarzkopf, J.J. Sirutis, W.F. Stern, M.J. Spelman, M. Winton, A.T. Wittenberg, B. Wyman (2006), GDFL's CM2 global coupled climate models. Part I: Formulation and simulation characteristics, *J. Clim*., 19, 643-674.

Flato, G.M. (2005), The Third Generation Coupled Global Climate Model (CGCM3). [Available online at http://www.cccma.bc.ec.gc.ca/models/cgcm3.shtml.]

Folland, C.K., and D.E. Parker (1990), Observed variations of sea surface temperature, *Climate-Ocean Interaction*, M.E. Schlesinger, Ed., Kluwer, 21-52.

Folland, C.K., and D.E. Parker (1995), Correction of instrumental biases in historical sea surface temperature data, *Quart. J. Roy. Meteor. Soc.*, 121, 319-367.

Gershunov, A., and T.P. Barnett (1998), Interdecadal modulation of ENSO teleconnections, *Bull. Am. Met. Soc.,* 79, 2715-2725.

Gordon, C., C. Cooper, C.A. Senior, H.T. Banks, J.M. Gregory, T.C. Johns, J.F.B. Mitchell, and R.A. Wood (2000), The simulation of SST, sea ice extents and ocean heat transports in a

version of the Hadley Centre coupled model without flux adjustments. *Climate Dyn*., 16, 147–168.

Hurvich, C.M., and C.L. Tsai (1989), Regression and time series model selection in small samples, *Biometrika,* 76, 297-307.

IPCC4 (2007), *Climate Change 2007: The Physical Science Basis. Contribution of Working Group I to the Fourth Assessment Report of the Intergovernmental Panel on Climate Change* [Solomon, S., D. Qin, M. Manning, Z. Chen, M. Marquis, K.B. Avery, M. Tignor and H.L. Miller (eds.)], Cambridge Univ. Press, Cambridge, UK.

Johns, T. C., and Coauthors, 2006: The new Hadley Centre climate model HadGEM1: Evaluation of coupled simulations. *J. Clim*., 19, 1327–1353.

Jones, P.D., T. Jonsson, and D. Wheeler (1997), Extension to the North Atlantic Oscillation using early instrumental pressure observations from Gibraltar and South-west Iceland, *Int. J. Climatol.*, 17, 1433-1450.

Kaplan, A., Y. Kushnir, and M.A. Cane (2000), Reduced space optimal interpolation of historical marine sea level pressure: 1854-1992, J. Clim., 13, 2987-3002.

Lapp, Suzan, Dave Sauchyn and Brenda Toth. 2009. Constructing scenarios of future climate and water supply for the SSRB: Use and limitations for vulnerability assessment. Prairie Forum, Special Issue, June, 2009.

Mantua, N.J., S.R. Hare, Y. Zhang, J.M. Wallace, and R.C. Francis (1997), A Pacific interdecadal climate oscillation with impacts on salmon production, *Bull. Amer. Meteorol. Soc.,* 78, 1069-1079.

Mantua, N.J., and S.R. Hare (2002), The Pacific Decadal Oscillation, *J. Oceanogr.,* 58, 35-44.

Martin, G.M., M.A. Ringer, V.D. Pope, A. Jones, C. Dearden, and T.J. Hinton (2006), The physical properties of the atmosphere in the new Hadley Centre Global Environmental Model (HadGEM1). Part I: Model description and global climatology. *J. Clim.*, 19, 1274–1301.

Min, S-K., Z. Xuebin, and F. Zwiers, (2008), Human-Induced Arctic Moistening, *Science*, 320, 518-520.

Minobe, S. (1997), A 50-70 year climatic oscillation over the North Pacific and North America, *Geophys. Res. Let.,* 24, 683-686.

Muller, W. A. and E. Roeckner (2006), ENSO impact on Midlatitude Circulation Patterns in Future Climate Change Projections. *Geophys. Res. Let.,* 33, DOI:10.1029/2005GL025032.

Nakicenovic N., J. Alcamo, G. Davis, B. de Vries, J. Fenhann, S. Gaffin, K. Gregory, A. Grübler, T.Y. Jung, T. Kram, E.L. La Rovere, L. Michaelis, S. Mori, T. Morita, W. Pepper, H. Pitcher, L. Price, K. Riahi, A. Roehrl, H.H. Rogner, A. Sankovski, M. Schlesinger, P. Shukla, S. Smith, R. Swart, S. van Rooijen, N. Victor, Z. Dadi (2000), IPCC Special

Report on Emissions Scenarios, Cambridge University Press, Cambridge, United Kingdom and New York, NY, USA.

Newman, M., G.P. Compo, and M.A. Alexander (2003), ENSO-forced variability of the Pacific Decadal Oscillation, *J. Clim.,* 16, 3853-3857.

Newman, M., (2007), Interannual to Decadal Predictability of Tropical and North Pacific Sea Surface Temperatures, *J. Clim.,* 20, 2333-2356.

Overland, J.E., and M. Wang (2007), Future climate of the North Pacific ocean, *Eos,* 88, 178, 182.

Pope, V.D., M.L. Gallani, P.R. Rowntree, and R.A. Stratton (2000), The impact of new physical parametrizations in the Hadley Centre climate model: HadAM3. *Climate Dyn*., 16, 123–146.

Rayner, N.A., D.E. Parker, E.B. Horton, C.K. Folland, L.V. Alexander, D.P. Rowell, E.C. Kent, and A. Kaplan (2003) Globally complete analyses of sea surface temperature, sea ice and night marine air temperature, 1871-2000, *J. Geophys. Res*. 108, 4407, DOI 10.1029/2002JD002670.

Reynolds, R.W., and T.M. Smith (1995), A high-resolution global sea surface temperature climatology, *J. Clim*., 8, 1571-1583.

Rood, S.B., G.M. Samuelson, J.K. Weber, and K.A. Wywrot (2005), Twentieth-century decline in streamflows from the hydrographic apex of North America, *J. Hydrol.,* 306, 215-233.

Rood, S.B., J. Pan, K.M. Gill, C.G. Franks, G.M. Samuelson, and A. Shepherd (2008), Declining summer flows of Rocky Mountain rivers: changing seasonal hydrology and probable impacts on floodplain forests, *J. Hydrol.,* 349, 397-410.

Ropelewski, C.F., and P.D. Jones (1987), An extension of the Tahiti-Darwin Southern Oscillation Index, *Mon. Weather Rev.,* 115, 2161-2165.

St. Jacques, J.M., D.J. Sauchyn and Y. Zhao (*in press*)*,* Northern Rocky Mountain streamflow records: global warming trends, human impacts or natural variability?, *Geophys. Res. Let.,* 2009GL042045.

Schindler, D.W., and W.F. Donahue (2006), An impending water crisis in Canada's western prairie provinces, *PNAS,* 103, 7210-7216.

Schneider, N., and B.D. Cornuelle (2005), The forcing of the Pacific Decadal Oscillation, *J. Clim.*, 18, 4355-4373.

Shabbar, A., and M. Khandekar, (1996), The impact of El Nino-Southern Oscillation on the temperature field over Canada. *Atmosphere-Ocean*, 34, 401-416.

Shabbar, A., B. Bonsal, and M. Khandekar (1997), Canadian precipitation patterns associated with the Southern Oscillation, *J. Clim.,* 10, 3016-3027.

Shabbar, A., and B. Bonsal, (2003), An Assessment of Changes in Winter Cold and Warm Spells over Canada. *Nat. Hazards*, 29, 173-188.

Shabbar, A., and W. Skinner (2004), Summer drought patterns in Canada and the relationship to global sea surface temperatures, *J. Clim.,* 17, 2866-2880.

Stewart, I., D.R. Cayan and M.D. Dettinger (2004), Changes in snowmelt runoff timing in western North America under a "business as usual" climate change scenario, *Clim. Change,* 62, 217-232.

Stewart, I., D.R. Cayan and M.D. Dettinger (2005), Changes toward earlier streamflow timing across western North America, *J. Clim.,* 18, 1136-1155.

Stoner, A.M.K., K. Hayhoe, and D.J. Wuebbles (2009), Assessing general circulation model simulations of atmospheric teleconnection patterns, *J. Clim.,* 22, 4348-4372.

van Vuuren, D.P. and K. Riahi (2008), Do recent emission trends imply higher emissions forever?, *Clim. Change,* 91, 237-248.

Wallace, J.M., and D.S. Gutzler (1981), Teleconnections in the geopotential height field during the Northern Hemisphere winter, *Mon. Weather Rev.*, 109, 784-812.

Wang, M., J.E. Overland, and N.A. Bond (2010), Climate projections for selected large marine ecosystems, *J. Mar. Sys.*, 79, 258-266.

Washington, W. M., and Coauthors, 2000: Parallel Climate Model (PCM) control and transient simulations. *Climate Dyn*., 16, 755–774.

Wilks, D.S. (2006), *Statistical Methods in the Atmospheric Sciences, 2nd ed.*, Academic Press, New York.

Woodward, W.A. and H.L. Gray (1993), Global warming and the problem of testing for trend in time series data, *J. Clim.,* 6, 953-962.

Yu, B. and F.W. Zwiers (2007), The impact of combined ENSO and PDO on the PNA climate: a 1,000-year climate modeling study, *Clim. Dyn.*, 29, 837-851.

Yu, B., A. Shabbar, and F.W. Zwiers (2007), The enhanced PNA-like climate response to Pacific interannual and decadal variability, *J. Clim.*, 20, 5285-5300.

Yukimoto, S. and Coauthors, (2001), The new Meteorological Research Institute global ocean-atmosphere coupled GCM (MRICGCM2)–Model climate and variability. *Pap. Meteor. Geophys.,* 51, 47–88.

Yukimoto, S., and A. Noda (2003), Improvements of the Meteorological Research Institute Global Ocean-Atmosphere Coupled GCM (MRI-GCM2) and its climate sensitivity. *CGER's Supercomputing Activity Rep.*, Vol. 10-2001, National Institute for Environmental Studies, Ibaraki, Japan, 37–44.

Zhang, X., K.D. Harvey, W.D. Hogg, and T.R. Yuzyk (2001), Trends in Canadian streamflow, *Water Resour. Res.,* 37, 987-998.

Zhang, Y., J.M. Wallace, and N. Iwasaka (1996), Is climate variability over the North Pacific a linear response to ENSO?, *J. Clim.,* 9, 1468-1478.

Zhang, Y., J.M. Wallace, and D.S. Battisti (1997), ENSO-like interdecadal variability: 1900-1993, *J. Clim.,* 10, 1004-1020.

Zheng, X., R.E. Basher, and C.S. Thompson (1997), Trend detection in regional-mean temperature series: maximum, minimum, mean, diurnal range, and SST, *J. Clim.,* 10, 317-326.

Zheng, X., and R.E. Basher (1999), Structural time series models and trend detection in global and regional temperature series, *J. Clim.,* 12, 2347-2358.